# SANDIA REPORT

SAND2014-16840
Unlimited Release
Printed August 2014

# Investigation of Wave Energy Converter Effects on Wave Fields: A Modeling Sensitivity Study in Monterey Bay, CA

Grace Chang, Jason Magalen, Craig Jones, and Jesse Roberts

Prepared by
Sandia National Laboratories
Albuquerque, New Mexico 87185 and Livermore, California 94550

Sandia National Laboratories is a multi-program laboratory managed and operated by Sandia Corporation, a wholly owned subsidiary of Lockheed Martin Corporation, for the U.S. Department of Energy's National Nuclear Security Administration under contract DE-AC04-94AL85000.



Sandia National Laboratories

Issued by Sandia National Laboratories, operated for the United States Department of Energy by Sandia Corporation.



Available to DOE and DOE contractors from
U.S. Department of Energy
Office of Scientific and Technical Information
P.O. Box 62
Oak Ridge, TN 37831

Telephone: (865) 576-8401
Facsimile: (865) 576-5728
E-Mail: reports@adonis.osti.gov
Online ordering: http://www.osti.gov/bridge

Available to the public from
U.S. Department of Commerce
National Technical Information Service
5285 Port Royal Rd.
Springfield, VA 22161

Telephone: (800) 553-6847
Facsimile: (703) 605-6900
E-Mail: orders@ntis.fedworld.gov
Online order: http://www.ntis.gov/help/ordermethods.asp?loc=7-4-0#online

SAND2014-16840
Unlimited Release
Printed August 2014

# Investigation of Wave Energy Converter Effects on Wave Fields: A Modeling Sensitivity Study in Monterey Bay, CA

Grace Chang, Jason Magalen, and Craig Jones
Sea Engineering, Inc.
200 Washington Street, Suite 101
Santa Cruz, CA 95060

Jesse Roberts
Water Power
Sandia National Laboratories
P.O. Box 5800
Albuquerque, New Mexico 87185-MS1124

**Abstract**

An industry standard wave modeling tool was utilized to investigate model sensitivity to input parameters and wave energy converter (WEC) array deployment scenarios. Wave propagation was investigated downstream of the WECs to evaluate overall near- and far-field effects of WEC arrays. The sensitivity study illustrated that both wave height and near-bottom orbital velocity were subject to the largest potential variations, each decreased in sensitivity as transmission coefficient increased, as number and spacing of WEC devices decreased, and as the deployment location moved offshore. Wave direction was affected consistently for all parameters and wave period was not affected (or negligibly affected) by varying model parameters or WEC configuration.

# ACKNOWLEDGMENTS

The research and development described in this document was funded by the U.S. Department of Energy. Sandia is a multiprogram laboratory operated by Sandia Corporation, a Lockheed Martin Company, for the United States Department of Energy's National Nuclear Security Administration under contract DE-AC04-94AL85000.

This research was made possible by support from the Department of Energy's Wind and Water Power Technologies Office.

# CONTENTS



# FIGURES

## TABLES

# NOMENCLATURE

| | |
|---|---|
| CCW | Counter clockwise |
| CDIP | Coastal Data Information Program |
| CW | Clockwise |
| DOE | Department of Energy |
| $H_s$ | Significant wave height |
| MWD | Mean wave direction |
| NDBC | National Data Buoy Center |
| NOAA | National Oceanic and Atmospheric Administration |
| NWW3 | WaveWatch III |
| PTO | Power take-off |
| SNL | Sandia National Laboratories |
| SWAN | Simulating WAves Nearshore |
| $T_p$ or $T_s$ | Peak wave period |
| WEC | Wave energy converter |

# 1. INTRODUCTION

In order to effectively convert wave energy into commercial-scale onshore electrical power, wave energy converter (WEC) devices need to be installed in arrays comprising multiple devices. The deployment of WEC arrays will begin small (pilot-scale or ~10 devices) but could feasibly number in the hundreds of individual devices at commercial-scale. As the industry progresses from pilot- to commercial-scale it is important to understand and quantify the effects of WECs on the natural nearshore processes that support a local, healthy ecosystem. WEC arrays have the potential to alter near-shore wave propagation and circulation patterns, possibly modifying sediment transport patterns and ecosystem processes. As WEC arrays sizes grow, there is a potential for negative environmental impacts which could be detrimental to local coastal ecology, and social and economic services. To help accelerate the realization of commercial-scale wave power, predictive modeling tools have been developed and utilized to investigate ranges of anticipated scenarios to evaluate the potential for negative (or positive) environmental impact.

The present study incorporates an industry standard wave modeling tool, SWAN (Simulating WAves Nearshore), to simulate wave propagation through a hypothetical WEC array deployment site on the California coast. Specifically, various sizes of WEC arrays are simulated to examine the changes to wave propagation properties (e.g. wave heights, periods and directions) in the lee of the array in both the near- and far-field. The study focuses on the change in wave properties resulting from variation in the ranges of SWAN model parameters, WEC array geometries, and array deployment locations (water depths).

At present, direct measurements of the effects of WEC arrays on wave properties for a prototype scale WEC site are not available; therefore, the effects of varying model parameters on the model results must be evaluated before environmental assessments can be completed. The present study provides the groundwork for completing such assessments by investigating the sensitivity of the predictive model results to prescribed model parameters over a range of anticipated wave conditions. The understanding developed here will allow investigators to conduct predictive environmental assessments with increased confidence and reduced uncertainty in future phases.

# 2. TECHNICAL APPROACH

Model sensitivity analysis was conducted using the wave propagation model SWAN, developed by the Delft Hydraulics Laboratory. Of particular interest was to understand model behavior (i.e. alterations to wave heights, periods and directions) in the vicinity of point absorber WEC devices and device arrays. Although only point absorber-type devices were studied here, the fundamental description of resultant model behavior will be beneficial to the study of all classes of WEC devices.

WEC devices will reflect and/or absorb differing amounts of wave energy depending upon device efficiency, device geometry, array configuration, and local wave conditions. Here, the modeled point absorber devices were represented within the SWAN model framework as "obstacles" to the propagating wave energy; the model allows specification of wave energy reflection and transmission coefficients at each obstacle, which denote the fraction of wave energy that is reflected and/or transmitted. The energy that is not transmitted or reflected is "absorbed" by the obstacle.

Prototype WEC devices have varying absorption and reflection properties which are, at present, largely unknown, uncertain, or unreported. Therefore, model behavior based on varying reflection and transmission coefficients was one of the foci of sensitivity analysis. Further, the effect of transmission coefficient variation along with additional model variations (number of WEC devices and WEC array deployment location [depth contour]) was investigated.

## 2.1. SWAN Model

As deep-water waves approach the coast, they are transformed by certain processes including refraction (as they pass over changing bottom contours), diffraction (as they propagate around objects such as headlands), shoaling (as the depth decreases), energy dissipation (due to bottom friction), and ultimately, by breaking. Since nearshore waves are the primary source of energy at the seabed in coastal settings, the accurate description of their propagation is a fundamental component in assessing nearshore circulation and sediment transport potential. The SWAN model has the capability of modeling all of these processes in shallow coastal waters.

The SWAN model is a non-stationary (non-steady state) third generation wave model, based on the discrete spectral action balance equation and is fully spectral (over the total range of wave frequencies). Wave propagation is based on linear wave theory, including the effect of wave generated currents. The processes of wind generation, dissipation, and nonlinear wave-wave interactions are represented explicitly with state-of-the-science third-generation formulations. Model boundary conditions can be explicitly specified by the user or may be obtained from nested, larger-domain modeling efforts (either SWAN or others such as WaveWatch III).

The SWAN model can also be applied as a stationary (steady-state) model. This is considered acceptable for most coastal applications because the travel time of the waves from the seaward boundary to the coast is relatively small compared to the time scale of variations in the incoming wave field, the wind, or the tide. SWAN allows for numerous output quantities including two

dimensional (frequency and direction) spectra, significant wave height, mean wave period, mean wave direction and bottom orbital velocities (due to wave oscillations). The SWAN model has been successfully validated and verified in laboratory and complex field cases elsewhere, and, as mentioned above, was determined acceptable for evaluation at this location as well (Booij et al., 1996).

### *2.1.1. Model Domain*

The selected modeling site was nearshore Monterey Bay and Santa Cruz, California. A previously validated SWAN model for the same region was used to propagate waves from deep-water offshore to shallow water (Chang et al., 2010). An offshore, coarser resolution grid model domain was nested with a finer resolution grid, near-shore model domain.

The model was in the Monterey Bay region using the National Oceanic and Atmospheric Administration (NOAA) National Data Buoy Center (NDBC) buoy data from within, and in proximity to, Monterey Bay. Several local NOAA NDBC buoys provided measurements of significant wave heights, dominant wave periods, peak wave directions, wind speeds and wind directions at the buoy locations dating as far back as 1987. These measured datasets were then compared to model output to demonstrate excellent model performance (Chang et al., 2010).

The two SWAN model grids (coarse and finer resolution) were nested to predict the propagation of deep-water waves from offshore of Monterey Bay, CA, to nearshore Santa Cruz, CA. The coarse grid (herein referred to as the Monterey Bay model domain) resolution was approximately 0.001° degrees in latitude and longitude (approximately 100 m grid spacing in x and y). The model was run as a stationary model: meteorological and hydrodynamic conditions at the offshore boundaries were kept constant. Directional wave energy spectra conditions were exported from the coarse resolution model and used as boundary conditions for the nested, fine resolution model (herein referred to as the Santa Cruz model domain).

The grid resolution of the nested Santa Cruz model domain computational grid was approximately 0.00025° degrees in latitude and longitude (approximately 25 m in x and y). The wave spectrum boundary conditions were applied along the offshore boundaries of the Santa Cruz SWAN model domain. The nested grid model was also implemented as a stationary model.

The Monterey Bay and Santa Cruz SWAN model domains are shown in Figure 1 (the inner dashed outline denotes the nested Santa Cruz model domain). NOAA NDBC buoys within the domain, used for validation, are noted. Data from NDBC buoy 46042 was used to derive Monterey Bay domain boundary conditions. Data from NDBC buoy 46236 were used to validate the model predictions for wave height, wave period and mean wave direction. Wave model validation is discussed in Chang et al. (2010).

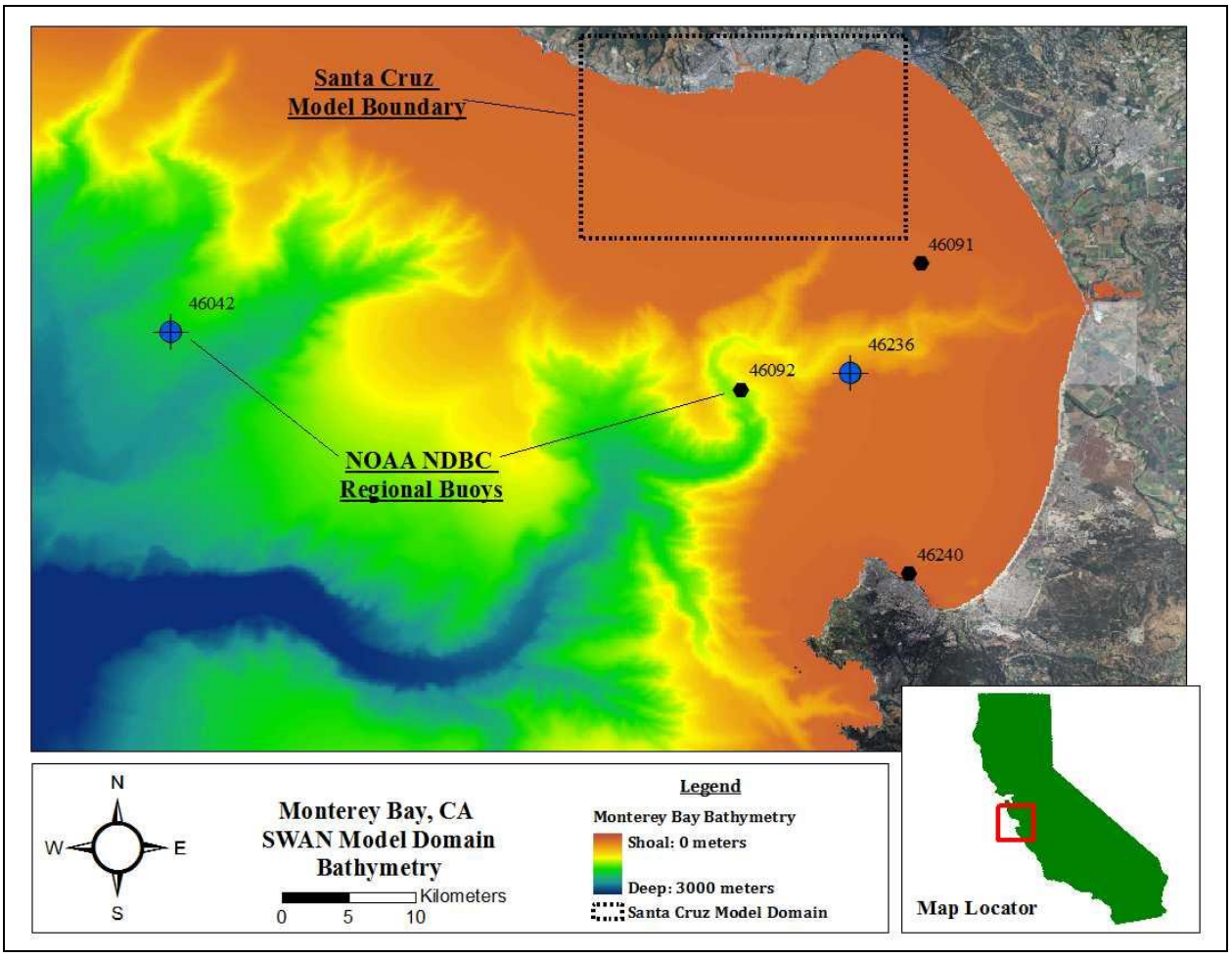


**Figure 1. Monterey Bay and Santa Cruz, CA, SWAN model domains. NOAA NDBC validation buoy locations are indicated.**

### *2.1.2. Boundary Conditions*

Historical wave conditions offshore of Monterey Bay are fairly well understood due to the existence of long-term wave data measurements from several NOAA NDBC and Coastal Data Information Program (CDIP) buoys. Representative data from NOAA NDBC buoy #46042 were utilized to determine typical wave conditions to be expected in the Monterey Bay region. The buoy is located 27 nautical miles west-northwest of Monterey, CA, in greater than 2000 meters water depth. Data have been recorded at this location since 1987, making it a statistically reliable source for evaluating typical (and extreme) wave conditions approaching Monterey Bay.

A wave height and wave period rose was generated by the historical data to evaluate the historical wave climate.[1] Significant wave height is the average of the highest 1/3 of wave

[1]Wave heights are the significant wave heights; the wave periods are the dominant wave periods. The wave directions are the mean wave direction, MWD, recorded by the buoy, and are the directions *from* which the waves approach.

heights on record. Dominant wave periods correspond directly to the frequency containing the largest amount of wave energy. Mean wave directions are the directions *from* which the dominant waves (waves corresponding to the dominant period) are approaching.

Figure 2 illustrates that the dominant wave direction (most frequently occurring) was from the northwesterly direction. The plots also indicate the most frequently occurring wave heights and wave periods (magnitude of color bands in plots). The basic statistics (of all available wave data from this buoy) that resulted from the wave data analysis are listed in Table 1. Figure 3, Figure 4, and Figure 5 show the statistical histograms of each wave property and provide a visual comparison to the model input values selected for the present modeling effort. It is evident that the majority of the waves approach the Monterey Bay region from the northwest (270 – 360 degrees True North) and that more than half of the waves on record comprised of wave heights of 2.0 meters or less and wave periods of less than 12 seconds.

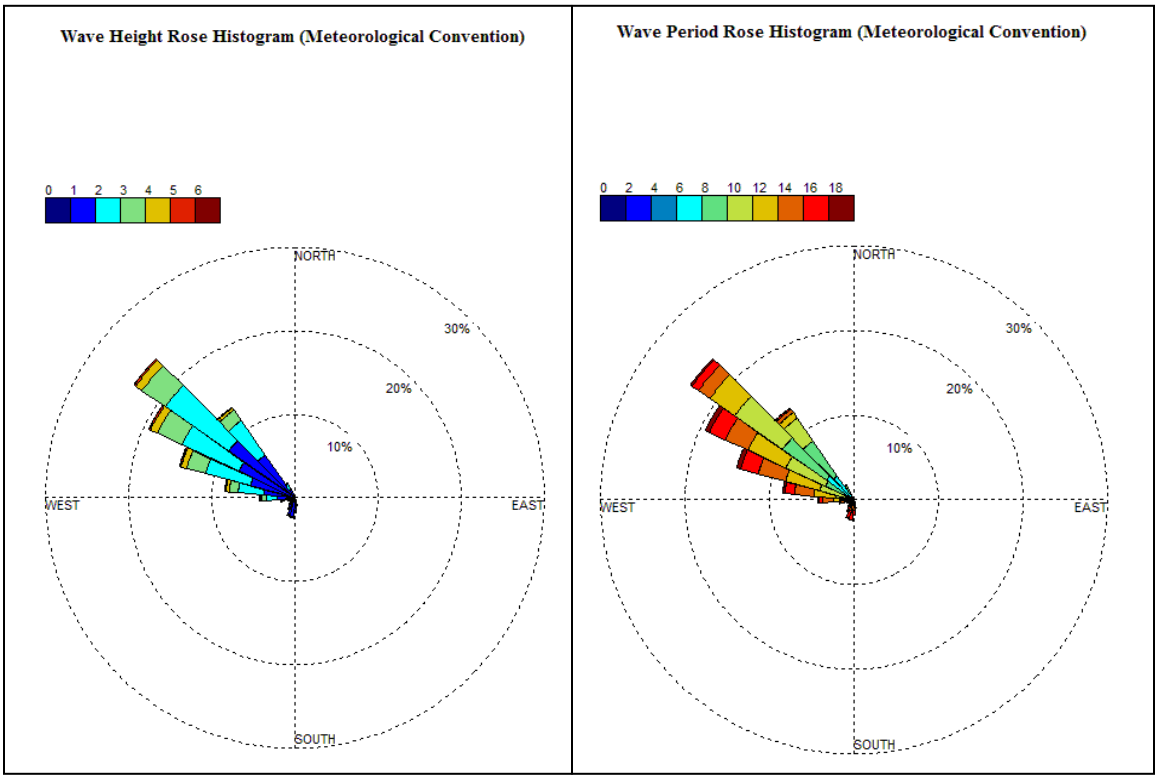


**Figure 2. Wave height (left) and wave period (right) rose diagrams showing direction *from* which the waves are approaching. Data collected by NOAA NDBC buoy #46042.**

**Table 1. Statistical data analysis - NOAA NDBC buoy #46042.**

| Parameter and Units | Mean Value | Median Value | Mode Value |
|---|---|---|---|
| $H_s$ (m) | 2.2 | 2.0 | 1.7 |
| $T_p$ (s) | 11.8 | 11.4 | 12.5 |
| MWD (degrees) | 287.5 | 299 | 310 |

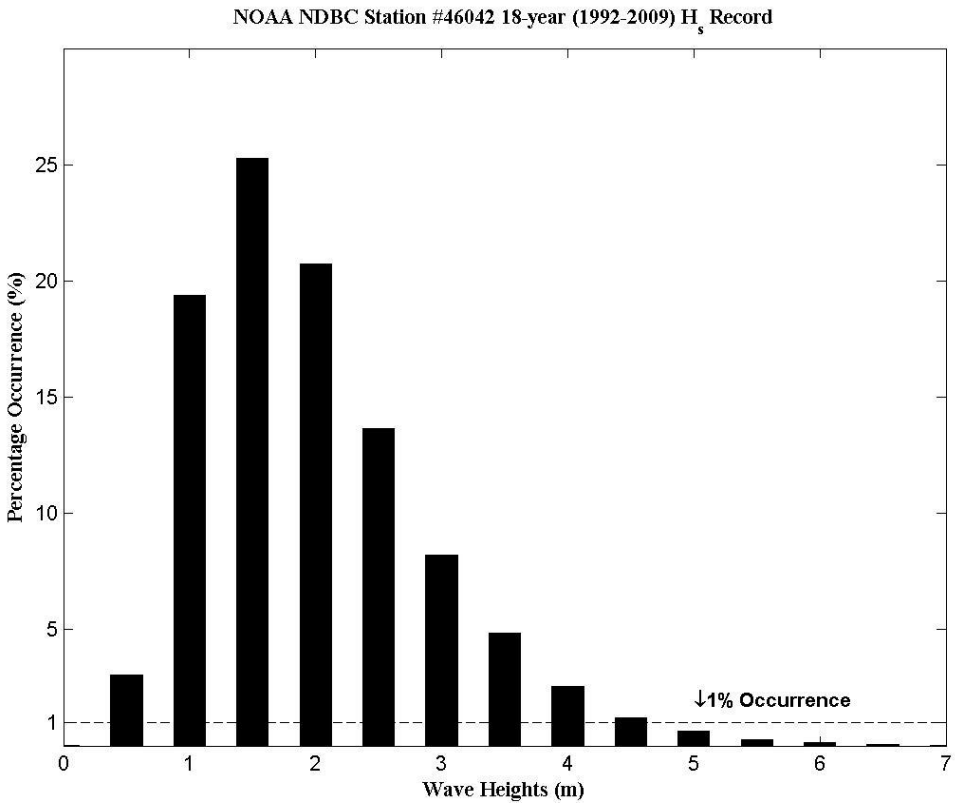


**Figure 3. Wave height histogram (frequency of occurrence) - NOAA NDBC buoy #46042.**

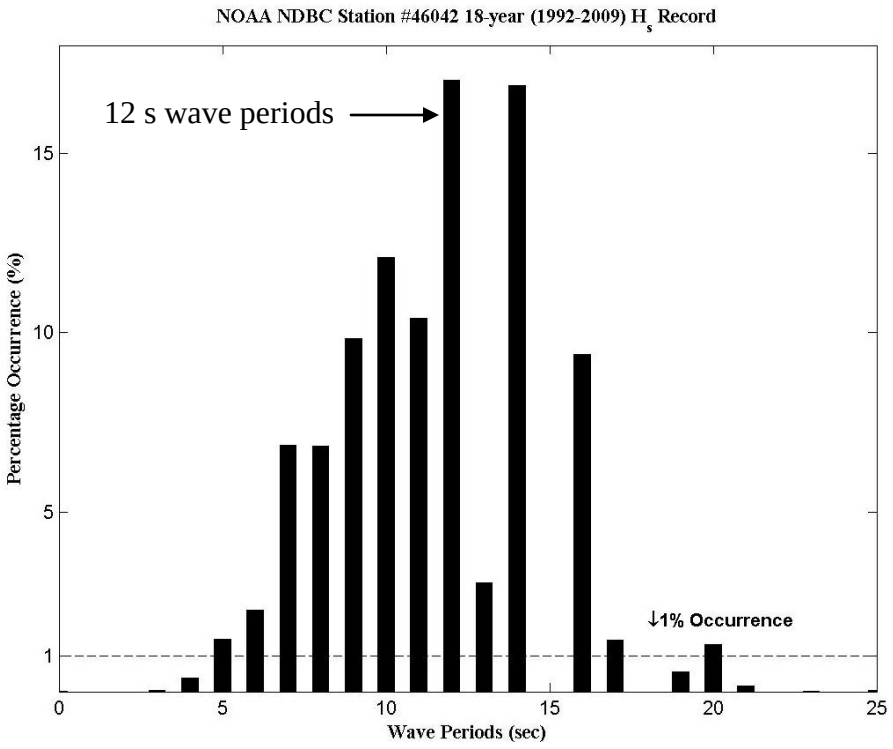


**Figure 4. Wave period histogram (frequency of occurrence) - NOAA NDBC buoy #46042.**

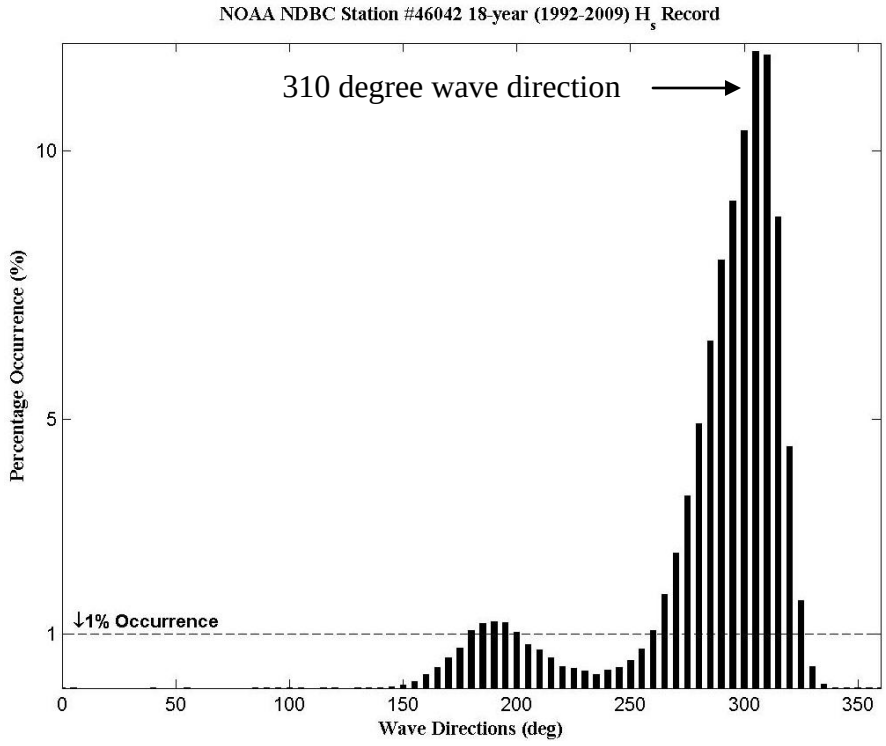


**Figure 5. Wave direction histogram (frequency of occurrence) - NOAA NDBC buoy #46042.**

In order to model a scenario with potential nearshore (and shoreline) Santa Cruz impacts, representative offshore wave conditions were selected based on their potential to alter nearshore wave properties. Based on the data analyzed from NOAA NDBC buoy #46042, two different sets of wave heights and periods: $H_s$ = 2.0 and 1.7 m, $T_p$ = 12.0 and 12.5 sec, respectively, were selected for representative offshore boundary conditions (Table 2). The offshore mean wave directions applied at the boundaries were 310 degrees and 205 degrees (Table 2), chosen because these caused wave shadowing to occur in the direction of the nearest shoreline (order 5 km) to the simulated WEC deployment locations (see Section 2.1.3 below).

**Table 2. Model Boundary Conditions.**

| Parameter (units) | Value 1 | Value 2 |
|---|---|---|
| $H_s$ (m) | 2.0 | 1.7 |
| $T_p$ (sec) | 12.0 | 12.5 |
| MWD (degrees) | 310 | 205 |

This was a conservative approach at modeling WEC array impacts on nearshore wave properties because waves approach Santa Cruz from a southwesterly direction (180° to 270° True North) approximately 15% of the time and waves approach the region from a northwesterly direction (270° to 360° True North) approximately 80% of the time. These simulations, however, illustrated the potential effects on wave properties near the Santa Cruz shoreline if a WEC array were to be installed in locations offshore of Santa Cruz (see Section 2.1.3 below).

Offshore model boundary conditions were specified for all "wet" boundaries (north, west and south sides) of the Monterey Bay domain. Waves were propagated from offshore to onshore throughout the entire domain. Wave frequency and directional spectra were extracted along the "wet" boundaries of the Santa Cruz domain and used as input boundary conditions for the nested, Santa Cruz domain (Figure 1). Waves were then propagated from the offshore boundaries of the Santa Cruz model domain to the shoreline.

### *2.1.3. Model Simulations with WECs*

In addition to modeled "baseline conditions" in which no obstacles to "absorb" wave energy were incorporated in SWAN (i.e. no WEC devices simulated), scenarios that included obstacles (i.e. simulated WECs) were modeled to investigate model sensitivity and to ascertain the effects of WECs on wave propagation. The Monterey Bay and Santa Cruz model domains were used to determine the changes in model predictions for different WEC array configurations as well as variable WEC reflection and transmission coefficients.

Within SWAN, reflection and transmission coefficients determine the amount of wave energy that is reflected by the obstacles or allowed to transmit past the obstacles. By varying these values, the effect of the WEC devices on reflection and absorption can be quantified. WEC absorption of energy was represented using constant transmission and reflection coefficients for

simplicity of evaluating the model sensitivity. The reflection or transmission filter was applied uniformly across all wave frequencies. While prototype WEC device power take-off (PTO) may be directly related to specific wave frequencies (i.e. WEC devices may be tuned to absorb more energy from specific frequencies), investigation of model sensitivity to frequency-dependent transmission coefficients was not an objective of the present study.

Two different model sensitivity analyses were performed:

- (Section 2.1.3.1) A 10-WEC device honeycomb array shape of variable separation distances in 50 m water depth southwest of Santa Cruz, CA (hereafter referred to as the honeycomb array WEC simulations) and
- (Section 2.1.3.2) Diamond-shaped device arrays of variable numbers of WECs and located at variable depths (hereafter referred to as the diamond-shaped array WEC simulations).

For all simulations, each WEC device was assumed to have a diameter of one grid cell (in this case, 25 meters). This ensured that the device effect on wave properties was represented in the model (in SWAN, obstacles must cross the direct line connecting two grid points in order to be represented in the model as a distinct obstacle). Devices were equally spaced in all directions for all simulations.

#### 2.1.3.1. Honeycomb Array WEC Simulations

The offshore model boundary conditions applied to the honeycomb WEC array simulations were: $H_s$ = 2.0 m, $T_p$ = 12.0 s, and MWD = 310 degrees (Value 1 in Table 2). Because of wave refraction by land in the western portion of the model domain, an initial offshore MWD of 310 degrees results in a nearshore MWD of 280 degrees. Therefore, the honeycomb array was oriented such that the broadest array dimension was perpendicular to the 280 degree direction (Figure 6). The wave direction rotation from that specified at the boundaries is a result of the effects of wave refraction. This configuration is a commonly proposed configuration for point absorbers. The setup yielded the most conservative estimate of changes in wave energy as a wider array footprint would "block" more wave energy from propagating past.

The honeycomb WEC array was located in approximately 50 meter water depth. Various device separation distances were evaluated and included 2.5 diameter (2.5X), 5 diameter (5X) and 10 diameter (10X) spacing. Diameter spacing was selected to evaluate a range of array geometries while still being able to resolve individual WEC devices in the model grid resolution.

In addition, SWAN model parameters, the frequency and directional spreading coefficients, were varied at the boundary of the computational grids (Monterey Bay and Santa Cruz domains) for investigation of their sensitivity within the honeycomb array WEC simulation (Table 3; Appendix A). Narrow-banded frequency and directional spectra (i.e. higher coefficient values) are akin to focused swell conditions (which are desired wave conditions by surfers). Wide-banded frequency and/or directional spectra (i.e. lower coefficient values) are typically more common and may indicate swell approaching from different directions or may indicate the

superposition of swell and locally generated wind-waves that are each approaching from different directions.

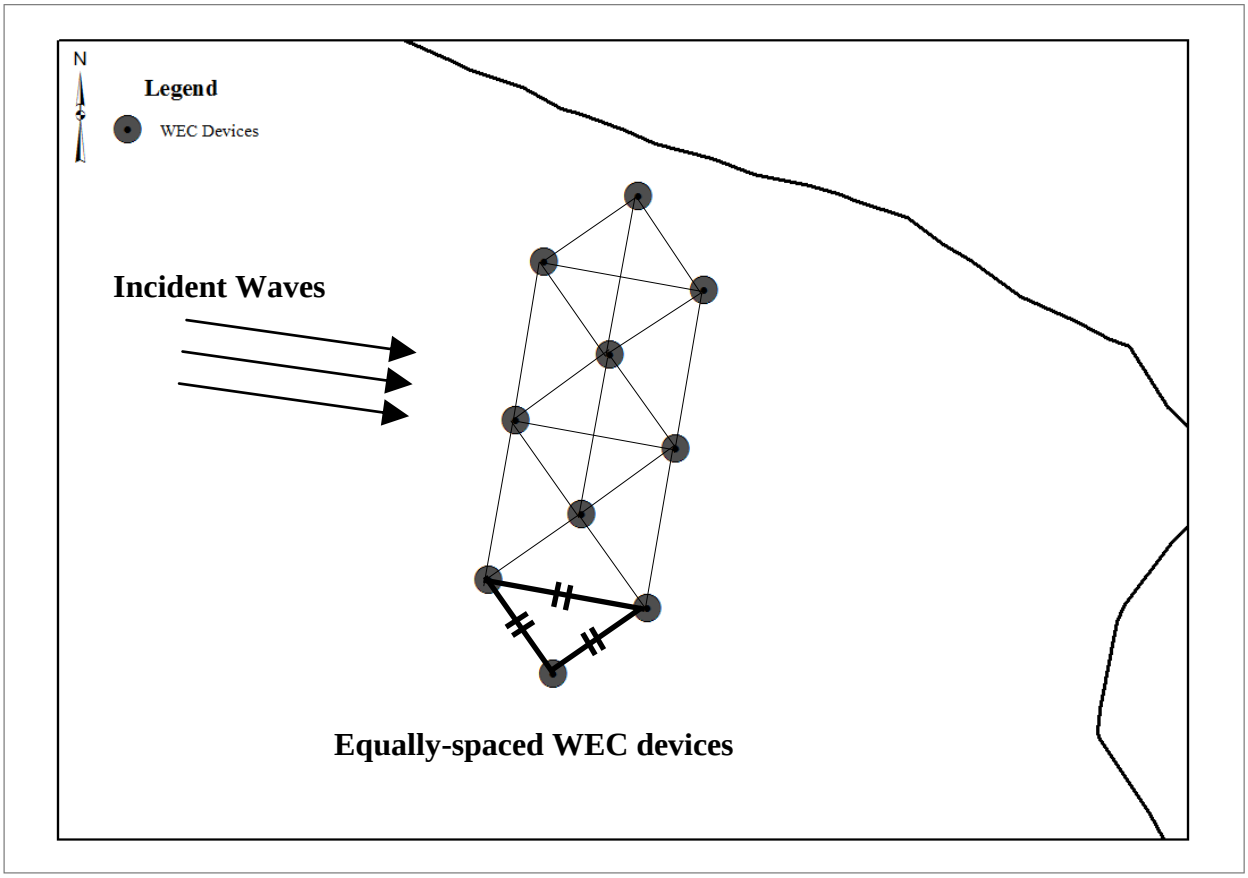


**Figure 6. Honeycomb geometry of WEC device arrays. The 50 m depth contour is shown as a solid black line.**

**Table 3. Sensitivity analysis parameter values for honeycomb WEC array simulations.**

| Coefficient or parameter | Value(s) |
|---|---|
| Transmission | [0.00, 0.25, 0.50, 0.75, 1.00] |
| Reflection | [0.00, 0.25, 0.50] |
| Frequency Spreading (gamma) | [1.0, 3.3, 10.0] |
| Directional Spreading (m) | [2.0, 10.0, 25.0] |
| WEC spacing (diameter) | [2.5X, 5X, 10X] |

Model output from honeycomb WEC array simulations was extracted from 15 locations (Table 4 and Figure 7 and Figure 8). Eight locations surrounded the simulated WEC array, each evenly

spaced from the WEC array centerline by 625 meters. This provided suitable model output locations for all array geometry spacing.

The other seven outputs were in the same locations for all array geometries to allow direct comparison of model predicted wave conditions. Four of these output locations were located 1 km, 5 km, 10 km and 20 km directly downstream of the center of the WEC array. Three near-shore locations were sited offshore of Point Santa Cruz (west of the wharf structure in 15 meters water depth), Santa Cruz beach (in 6 meters of water depth), and offshore of Pleasure Point (east of the wharf structure in 6 meters water depth). These are popular surfing locations, with surf breaks extending all the way around the points into the beaches at Santa Cruz. Changes in wave conditions due to the WEC array, if any, are important to ascertain at this location since this will concern the surfing community.

**Table 4. SWAN model output locations for honeycomb WEC array simulations.**

| Output Location Number | Description |
|---|---|
| 1 | Upstream – Offshore |
| 2 | Upstream – Centerline |
| 3 | Upstream – Onshore |
| 4 | Side – Offshore |
| 5 | Side – Onshore |
| 6 | Downstream – Offshore |
| 7 | Downstream – Centerline |
| 8 | Downstream – Onshore |
| 9 | Downstream – Centerline 1 km |
| 10 | Downstream – Centerline 5 km |
| 11 | Downstream – Centerline 10 km |
| 12 | Downstream – Centerline 20 km |
| 13 | Nearshore – Point Santa Cruz |
| 14 | Nearshore – Santa Cruz Beach |
| 15 | Nearshore – Pleasure Point |

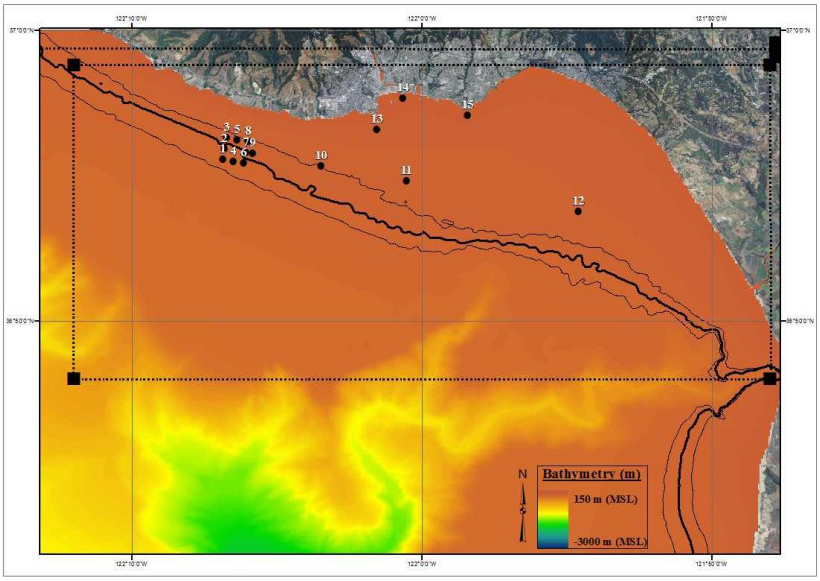


**Figure 7. Nested Santa Cruz domain showing honeycomb WEC array model output locations.**

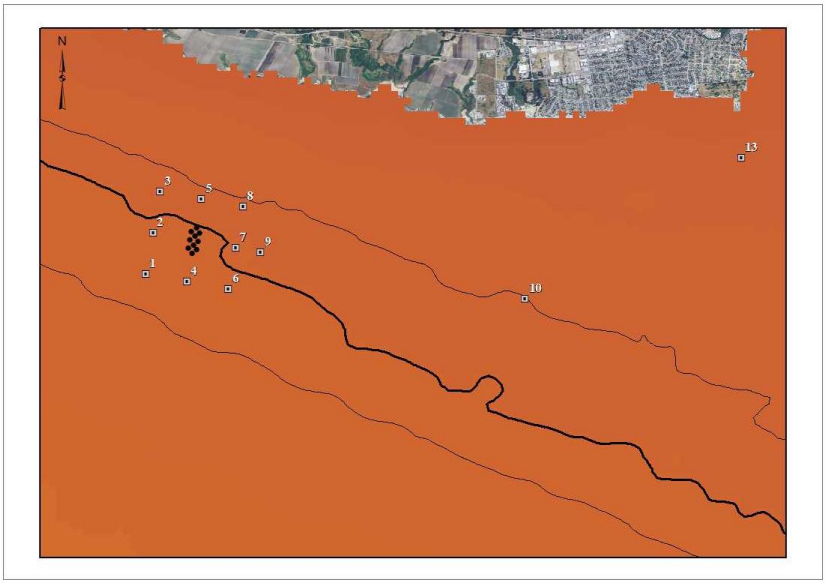


**Figure 8. Expanded view of WEC device honeycomb WEC array (black dots) and model output locations in proximity.**

### 2.1.3.2. Diamond-Shaped Array Simulations

In order to further evaluate the effects of WEC configuration on nearshore wave propagation, variations in the number of WEC devices in a diamond-shaped array (Figure 9) and the array deployment location (depth contour) were investigated. Larger numbers of WEC devices within

an array may "absorb" a larger amount of wave energy, resulting in a larger wave shadow in lee of the array (both in horizontal extent and in magnitude of wave decrease). Further, the WEC device array may have a more significant impact on shorelines in the lee of WEC arrays depending upon the depth contour at which the array is centered (i.e. the proximity of the shoreline to the WEC array). The full impact will depend on the depth at which the array is located as well as the bathymetry in the lee of the array (i.e. mild- versus steep-sloped bathymetry or large degree of elevation relief in at the lee of an array at which the wave refractive effects may be altered).

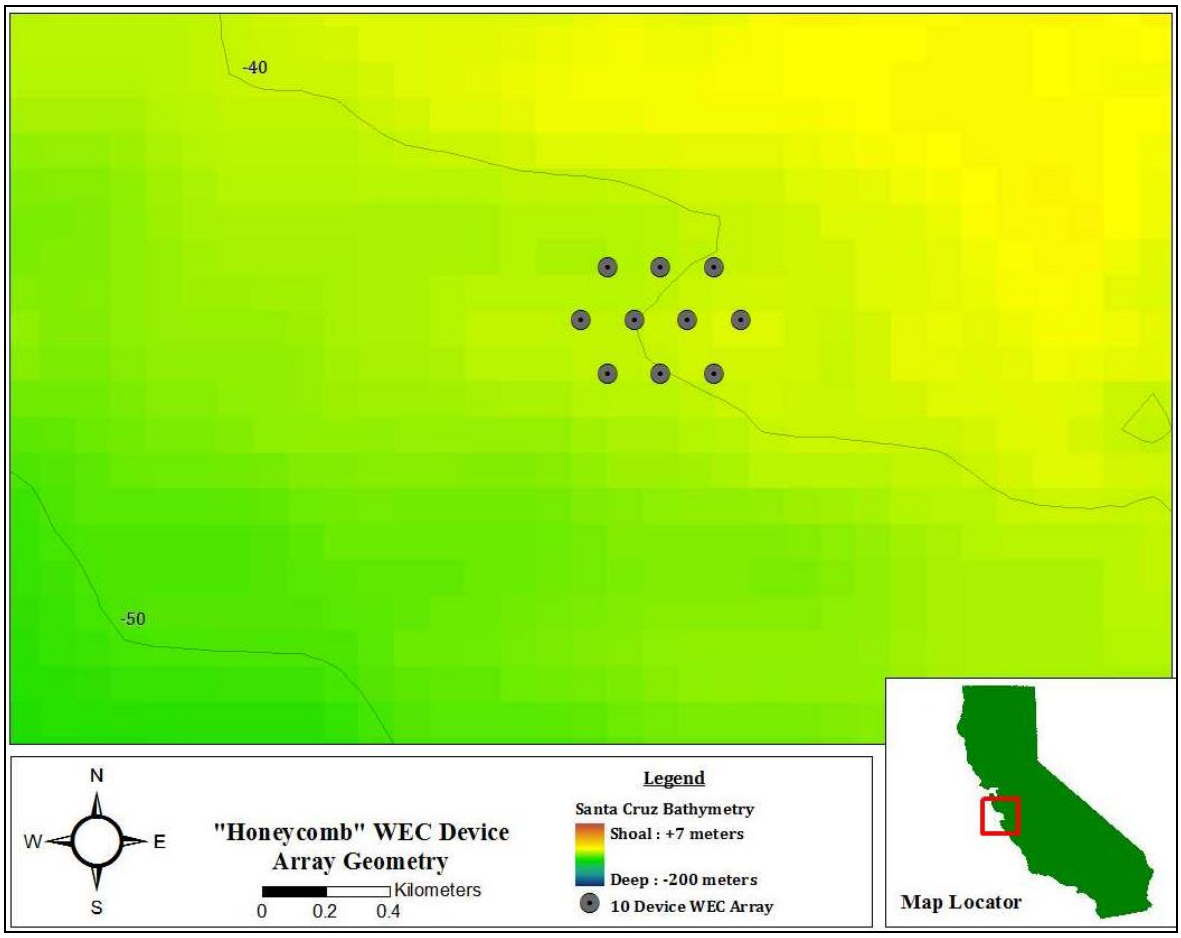


**Figure 9. Example diamond-shaped geometry of a 10-WEC device array in the model. The 40 m and 50 m depth contours are shown for reference.**

Diamond-shaped WEC array model sensitivity analysis parameters are listed in Table 5. The WEC array device numbers were varied between 10, 50, 100 and 200 WEC devices and the array locations were centered on the 40 meter, 50 meter, or 60 meter depth contours south of Santa Cruz, CA. WEC devices were simulated in the model with 6-diameter spacing between devices, center to center for diamond-shaped arrays. The transmission coefficient was varied between 0.3 and 0.7. For each scenario, one transmission coefficient, one WEC array deployment location

(depth contour), and one array size (number of devices) was selected. For brevity, Figure 10 shows an example of a 10-WEC array centered on three different depth contours: 40 m, 50 m, and 60 m. Figure 11, Figure 12, Figure 13, and Figure 14 illustrate the 10-, 50-, 100- and 200-WEC arrays centered on the 40 m contour. These are the sample model setups for each of the respective diamond-shaped WEC array wave modeling scenarios. Appendix B lists the total number of runs and the parameter values corresponding to each run.

**Table 5. Sensitivity analysis parameter values for diamond-shaped WEC array simulations.**

| Parameter | Values |
|---|---|
| Transmission Coefficient (Fraction of Wave Energy Allowed to Pass) | [0.3, 0.4, 0.5, 0.6, 0.7] |
| WEC Location (Depth Contours) | [40 m, 50 m, 60 m] |
| WEC Array Size (# Devices) | [10, 50, 100, 200] |

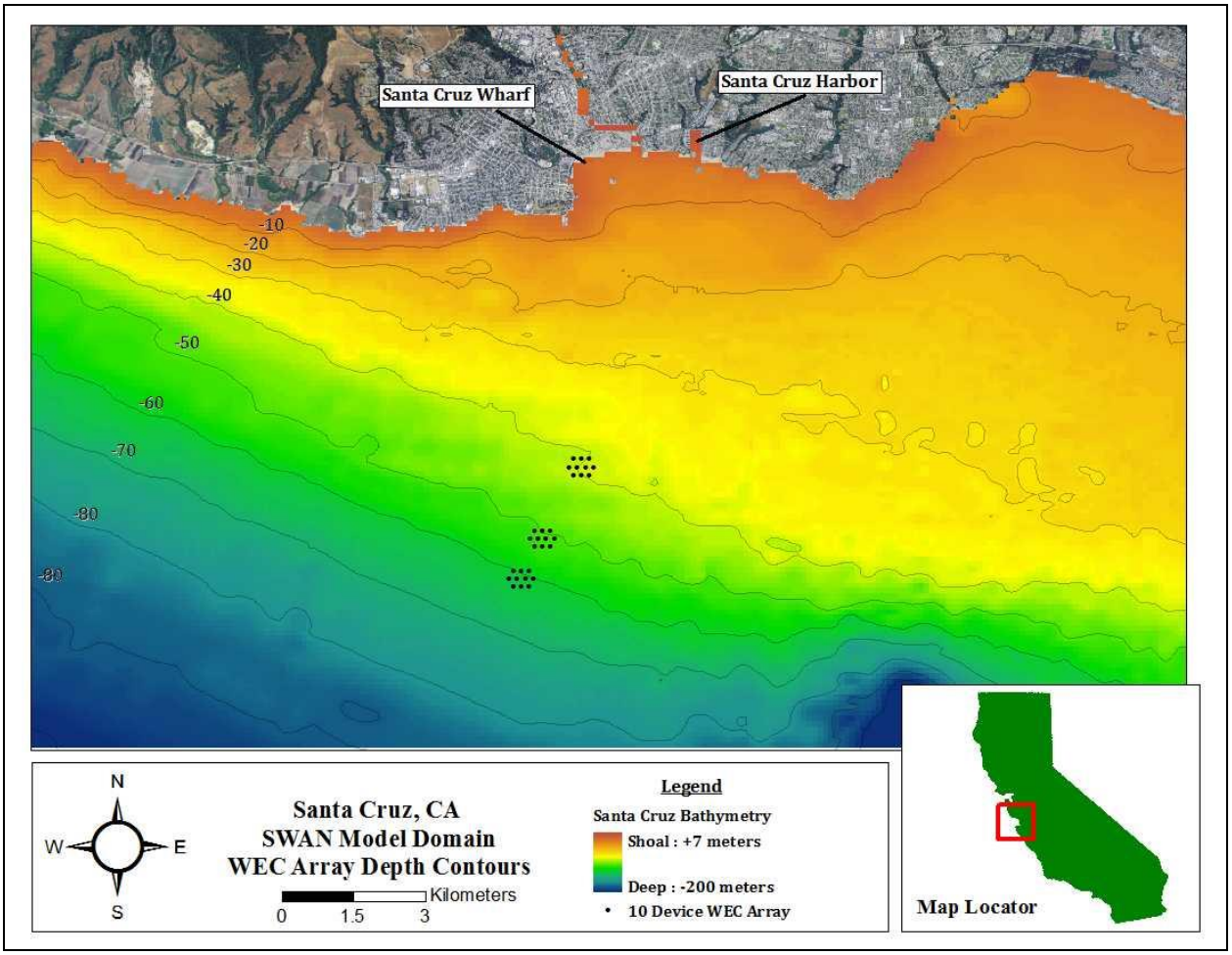


**Figure 10. Diamond-shaped arrays of 10-WEC devices centered on three different depth contours: 40 m, 50 m and 60 m.**

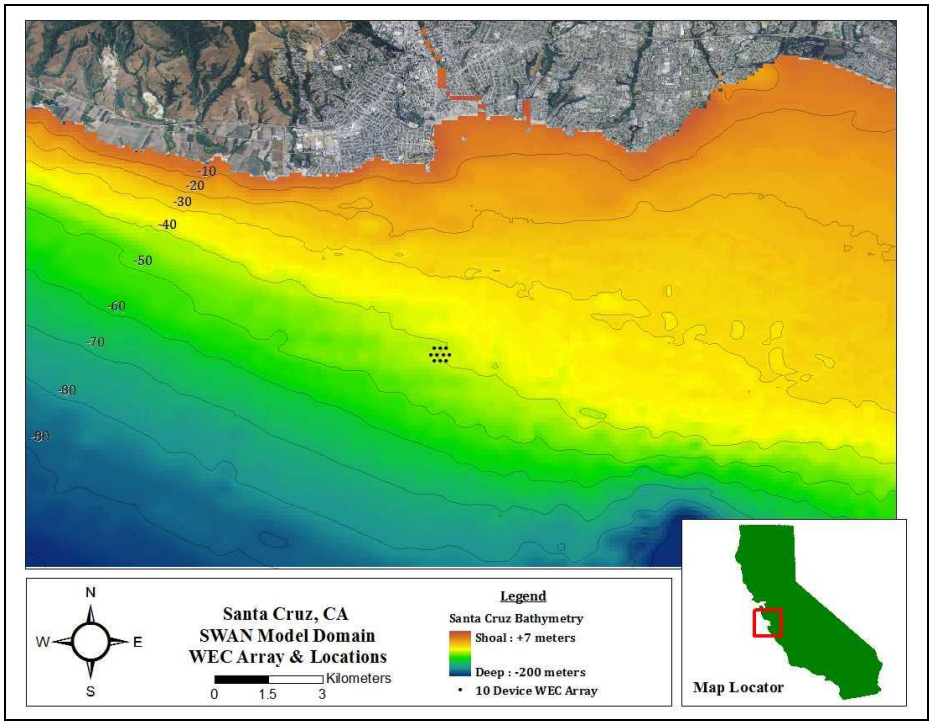


**Figure 11. A diamond-shaped array of 10-WECs centered on the 40 m depth contour.**

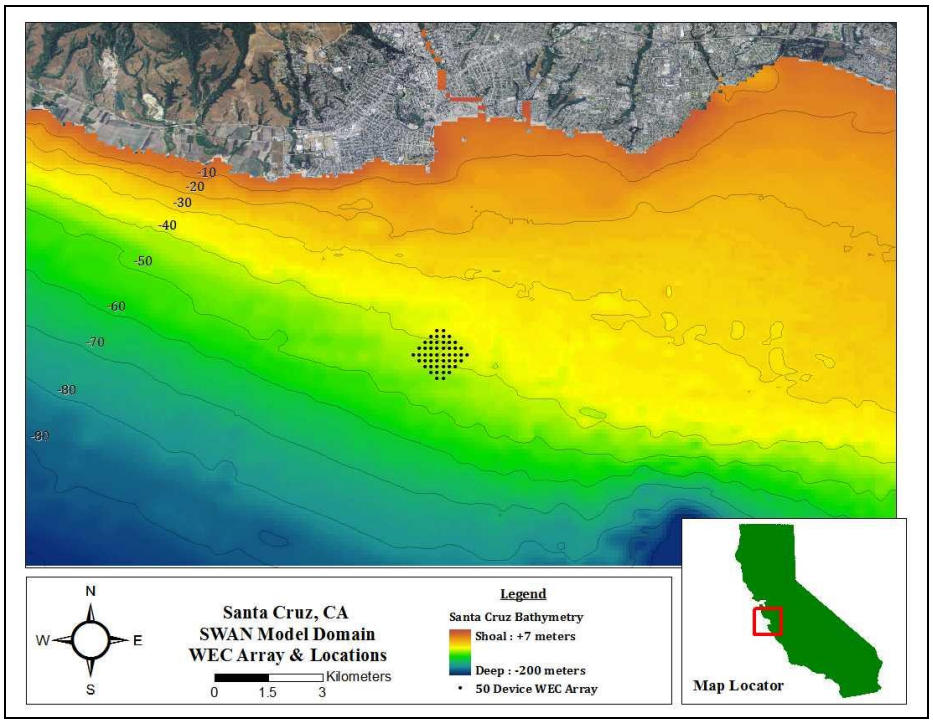


**Figure 12. A diamond-shaped array of 50-WECs centered on the 40 m depth contour.**

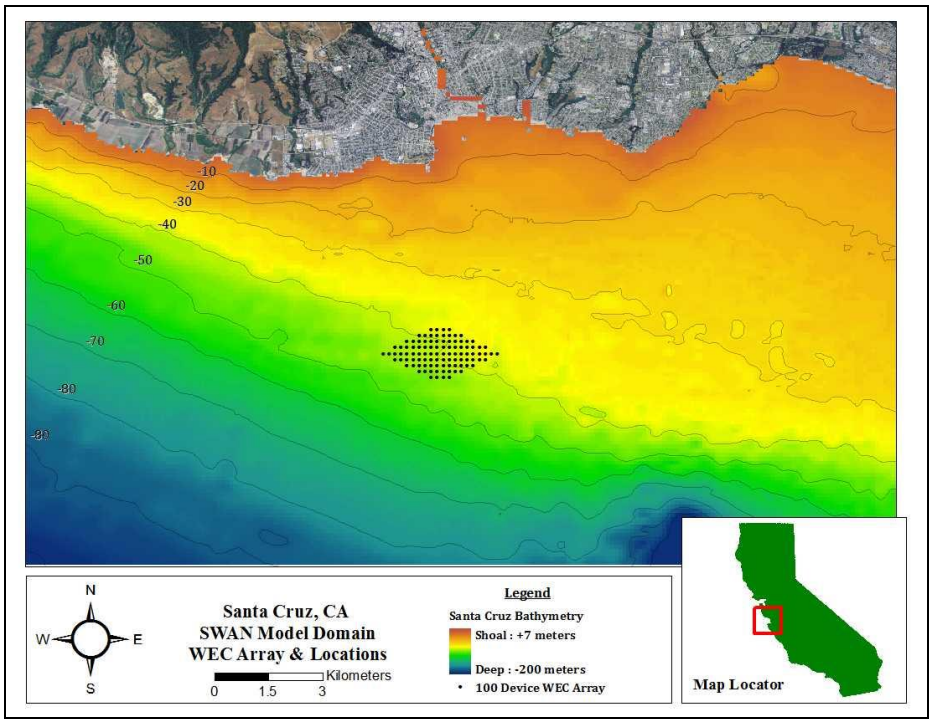


**Figure 13. A diamond-shaped array of 100-WECs centered on the 40 m depth contour.**

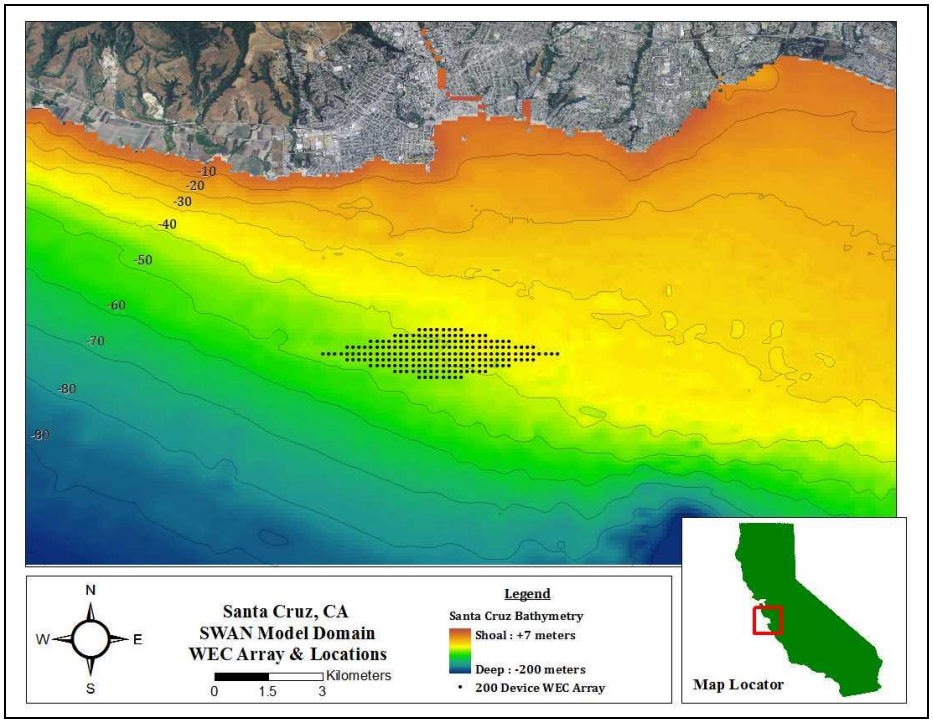


**Figure 14. A diamond-shaped array of 200-WECs centered on the 40 m depth contour.**

Model output for diamond-shaped WEC array simulations was extracted from 18 distinct locations (Table 6 and Figure 15). Model output extraction occurred at three depth contours offshore of each shoreline location: the 30 m, 20 m and 10 m depth contours, oriented and numbered sequentially south to north (see Figure 15). Six shoreline locations along the Santa Cruz coast were selected to span the anticipated horizontal extent of wave shadowing due to the WEC arrays (west to east):

- West Santa Cruz
- Steamer Lane
- Santa Cruz Wharf
- Santa Cruz Harbor
- East 26$^{th}$ Ave.
- Pleasure Point

These sections of the Santa Cruz shoreline are popular sight-seeing, surfing and recreation locations, with surf breaks, jogging paths and residential homes extending along the headlands and the beaches. Changes in nearshore wave conditions due to the WEC array, if any, are important to ascertain at this location since this will likely concern the recreational community. Furthermore, changes in wave conditions at these nearshore locations are important to evaluate from the perspective of tidal circulation, shoreline erosion, and ecological change.

**Table 6. Model output locations for diamond-shaped WEC array simulations.**

| Output Location Number | Depth Contour and Description | Output Location Number | Depth Contour and Description |
|---|---|---|---|
| 1 | 30 m - West Santa Cruz | 10 | 30 m – Santa Cruz Harbor |
| 2 | 20 m - West Santa Cruz | 11 | 20 m – Santa Cruz Harbor |
| 3 | 10 m - West Santa Cruz | 12 | 10 m – Santa Cruz Harbor |
| 4 | 30 m - Steamer Lane | 13 | 30 m – East 26th Ave |
| 5 | 20 m - Steamer Lane | 14 | 20 m – East 26th Ave |
| 6 | 10 m - Steamer Lane | 15 | 10 m – East 26th Ave |
| 7 | 30 m – Santa Cruz Wharf | 16 | 30 m - Pleasure Point |
| 8 | 20 m – Santa Cruz Wharf | 17 | 20 m - Pleasure Point |
| 9 | 10 m – Santa Cruz Wharf | 18 | 10 m - Pleasure Point |

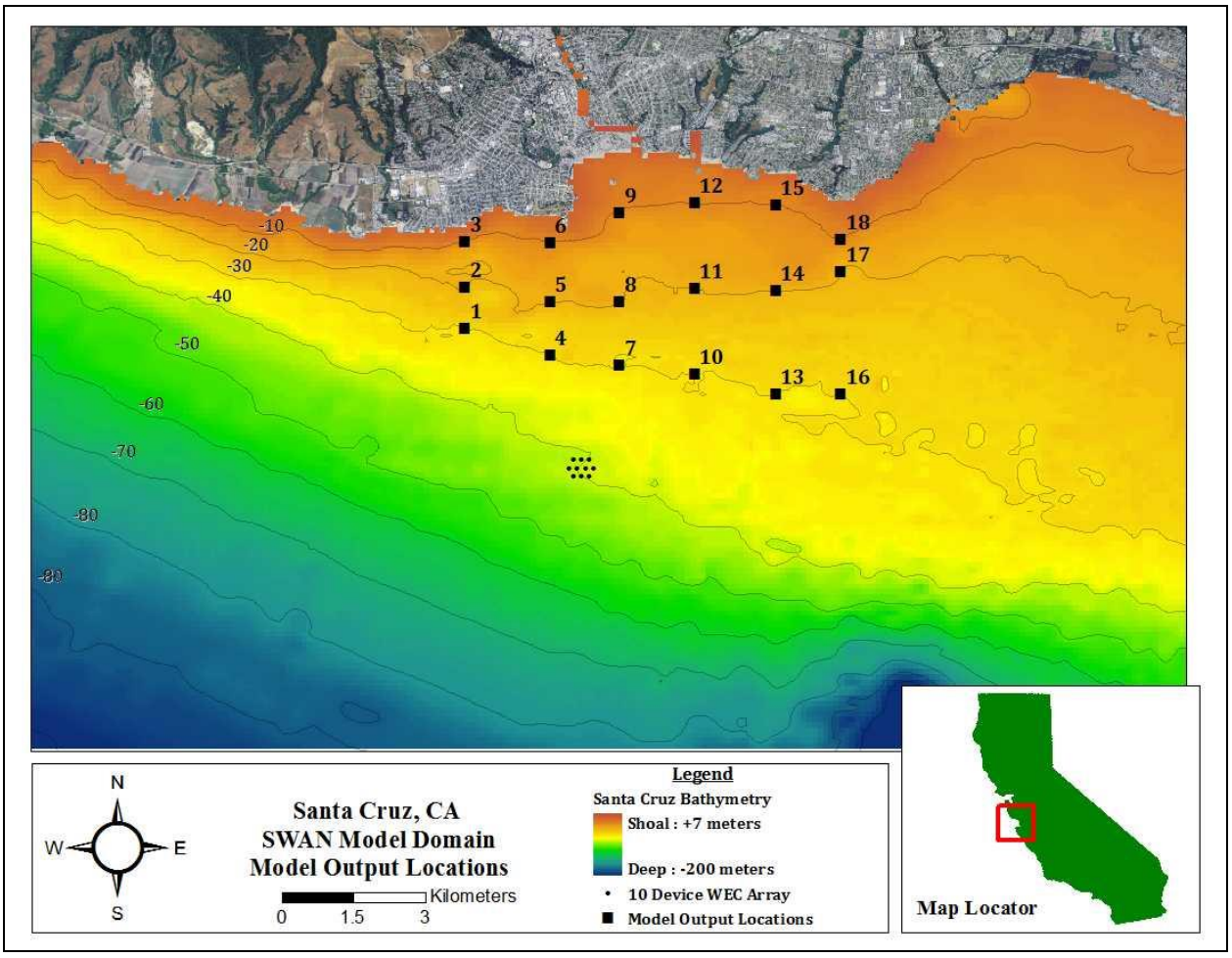


**Figure 15. Nested Santa Cruz domain with example diamond-shaped WEC device array on the 40 m depth contour. The numbered model output locations (black squares) are shown.**

# 3. RESULTS AND DISCUSSION

Results presented herein include propagated wave heights, wave periods and wave directions at all grid points in the domain.

## 3.1. Honeycomb WEC Array Simulation Results

Figure 16, Figure 17, **Error! Reference source not found.**, and **Error! Reference source not found.** display example wave height predictions from a baseline condition (no WEC devices) and three non-baseline conditions (incorporating WEC devices: 2.5X, 5X, and 10X WEC device spacing, respectively). **Error! Reference source not found.** is an expanded view of the wave height predictions at the WEC 5X spacing array that illustrates the wave height decreased in the lee as a result of "blocked" wave energy. All scenarios shown were modeled with: transmission coefficient of 0.0 (wave energy completely blocked at WEC device), a reflection coefficient of 0.0 (no wave energy reflection at WEC device), a frequency spreading coefficient of 10 ("peakier" spectral shape representative of swell conditions) and a directional spreading coefficient of 10 (narrow spreading, more focused waves).

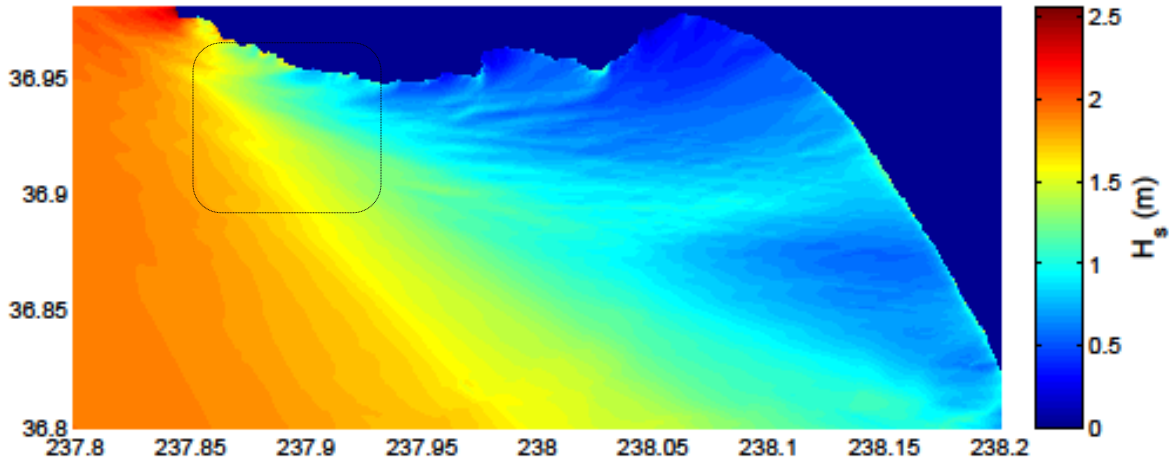


**Figure 16. Model wave height results from *baseline* condition (no WECs simulated). The dashed outline indicates the locations of the WEC array and model output points.**

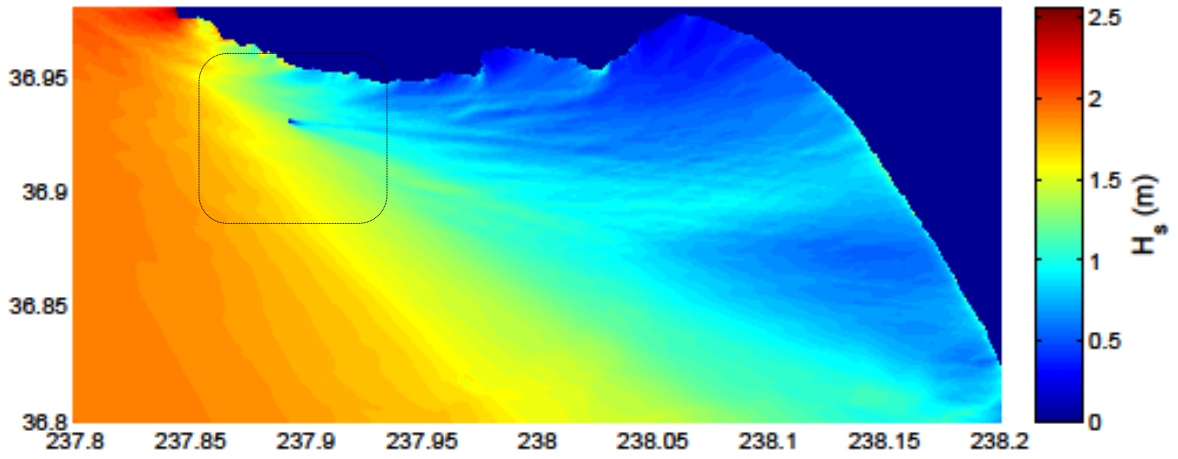


**Figure 17. Model wave height results from 2.5X WEC spacing condition.**

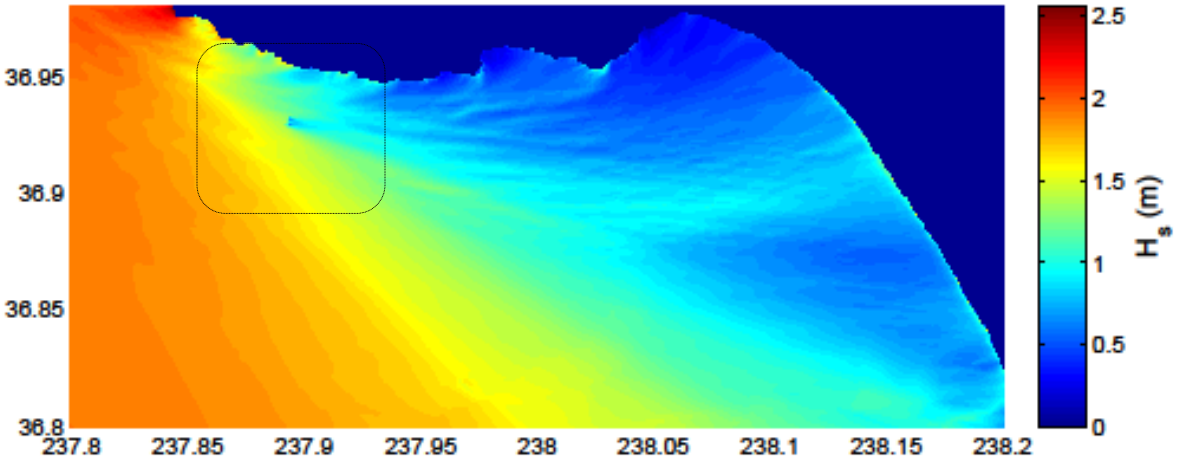


**Figure 18. Model wave height results from 5X WEC spacing condition.**

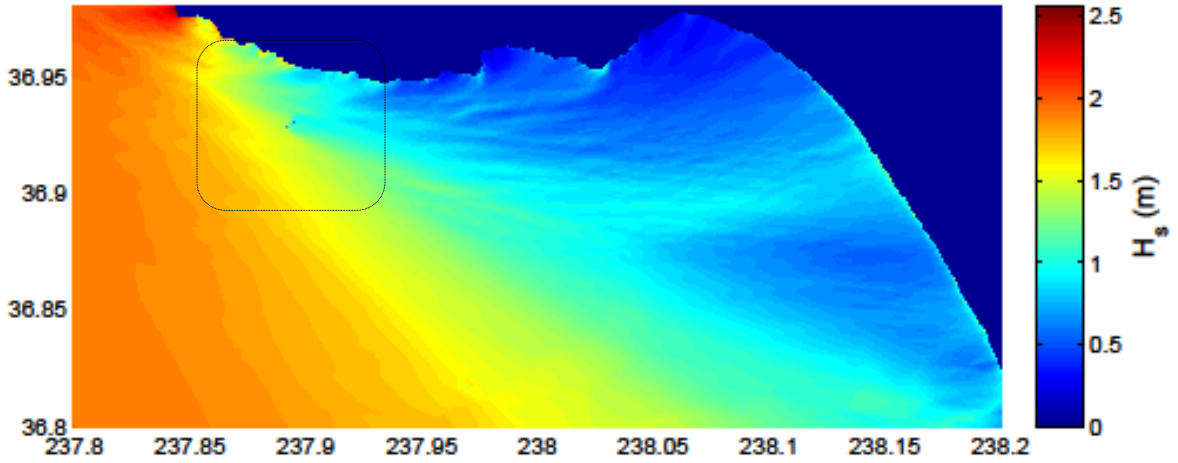


**Figure 19. Model wave height results from 10X WEC spacing condition.**

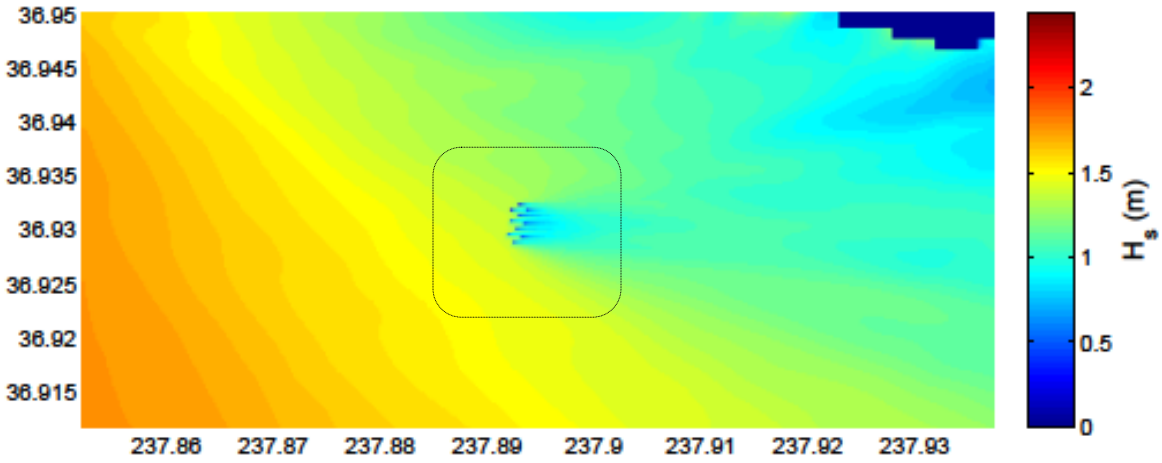


**Figure 20. Expanded view of model wave height results from 5X WEC spacing condition.**

Immediately evident from examination of Figure 17 through Figure 19 is that array device spacing had an effect on downstream wave conditions, both near-field and far-field. Based on visual observation, closer spacing of WEC devices (e.g. 2.5X) resulted in a larger decrease in wave energy propagation near the array compared to larger spaced arrays (5X or 10X spacing); The far-field effect of a closer-spaced array on the wave conditions was not as significant as larger-spaced arrays. However, to truly evaluate the far-field effects of the device spacing, the differences in wave conditions at the model output locations need to be quantified.

To facilitate this, the model output wave heights, wave periods and wave directions from each model run was compared individually to the baseline scenario model predictions. One at a time, the four sensitivity variables were held constant while the others were allowed to vary. The resulting differences in each wave condition were plotted for observation.

Figure 21 is an example scatter plot of percentage wave height differences at model output location 7 (downstream centerline of the array; see Table 4). Negative percentage indicates a wave height that has decreased in value from the baseline scenario value (due to absorbed, reflected or blocked wave energy). Each subplot denotes the model scatter that results from holding a particular sensitivity parameter constant while allowing the remaining parameters to vary. Clockwise from the top left, the sensitivity parameters held constant in each subplot are: transmission coefficient, reflection coefficient, directional spreading factor and the frequency spreading factor.

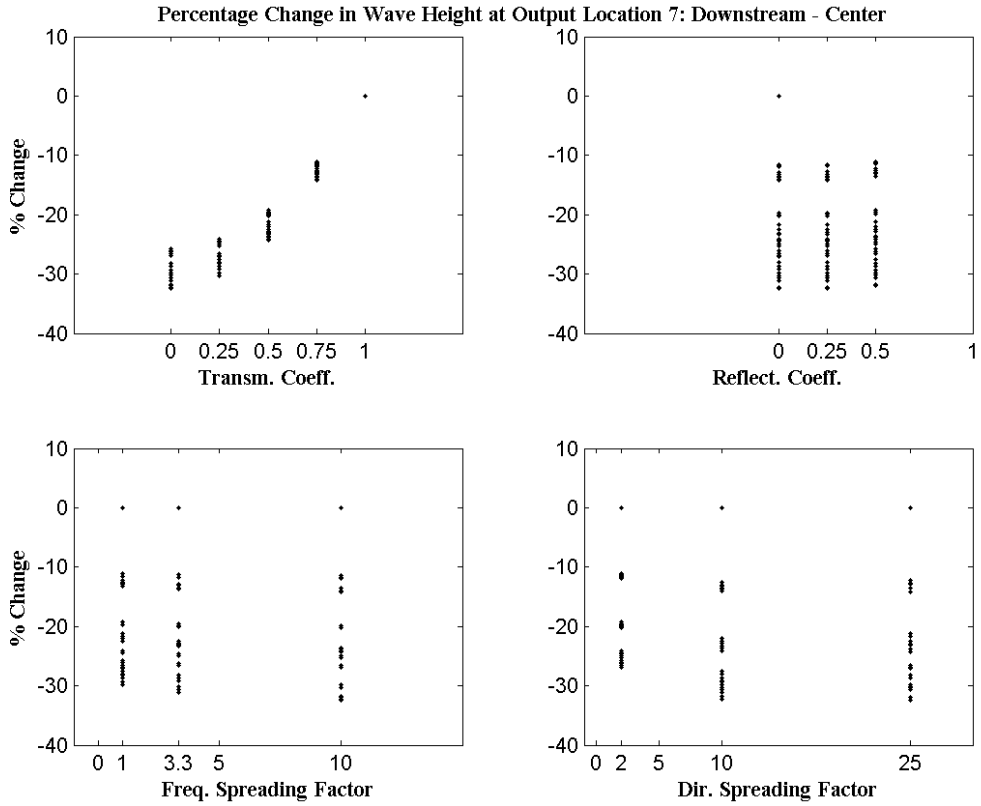


**Figure 21. Sensitivity analysis scatter plot for the 5X device spacing and model output location 7: Downstream Centerline. Each subplot represents a sensitivity analysis for a constant variable.**

The shape of the resulting scatter plot and degree of vertical spreading that existed for each constant parameter were indications of the model sensitivity to that parameter. For example, setting the transmission coefficient to zero (top left subplot in Figure 21) and allowing all other sensitivity parameters to vary resulted in a minimum decrease in wave height of ~25% and a maximum decrease in wave height of ~35% (vertical maximum and minimum for a transmission coefficient equal to 0).

On the other hand, by holding the frequency spreading factor constant to 1, 3.3 or 10 (bottom left Figure 21), a wide range of values resulted, from a 0% to ~30% decrease in wave height at this location, irrespective of the value of frequency spreading parameter chosen. This indicated that the model results were not very sensitive to the selected frequency spreading factor. In other words, the other varying parameters (e.g. transmission coefficient) had a much larger effect on wave heights.

Figure 21 ultimately illustrates that the model results were most sensitive to the transmission coefficient at this downstream location. Similar evaluations were made for the wave periods and wave directions modeled at each output location (see Appendix A). In general, wave period decreases were also sensitive to the transmission coefficient, and to a lesser degree, the directional spreading factor (lower directional spreading coefficient resulted in less scatter in model prediction). Wave direction was not as sensitive to changes in the coefficients as the other wave parameters (changes were small or negligible between baseline and array scenarios). Some changes were observed; however, additional analysis is required to fully explain the model sensitivity of mean wave direction to the varying of the parameters.

To summarize, model output locations upstream and to the sides of the array showed little to no change in wave heights compared to the baseline scenario. The largest wave height differences were observed downstream of the array along the array centerline (output locations 7 and 9). As distance downstream of the array increased (output locations 10 to 12), wave height percentage change decreased in magnitude as the effects of wave energy absorption and diffraction were mitigated.

Wave period changes at most model output locations were negligible (less than 0.5%). At nearby downstream array centerline locations, however, wave period decreased up to 8% from the baseline scenario. This amounted to a 1 second decrease in wave period for a 12 second incident wave and may be more of a result of the frequency bin spacing selected for model input than a decrease in wave period. Further evaluation is needed to fully explain the decrease in wave periods resulting from wave energy absorption.

Wave directional changes were also largely negligible (zero change) at most model output locations. For the downstream centerline locations, however, wave direction decreased up to 15 degrees (counterclockwise rotation of wave direction). The reason for this was not immediately clear and may be a result of several factors: natural wave refraction combined with a large directional spreading parameter in the wave spectrum. Furthermore, it may also have been a consequence of the directional bin spacing selected for model input.

### *3.1.1. Comparisons to WEC Device Spacing*

Similar comparisons were made between different WEC device array spacings to identify the effect the spacings had on both near- and far-field wave conditions. Figure 22 illustrates the percentage change in wave height between the 10X spacing and 2.5X spacing arrays at model location 7. In addition, the percentage change in wave height at model output location 10, (5 km downstream), is shown in Figure 23. A negative percentage means that the 10X case had a lesser effect on wave heights than the 2.5X by the negative percentage listed.

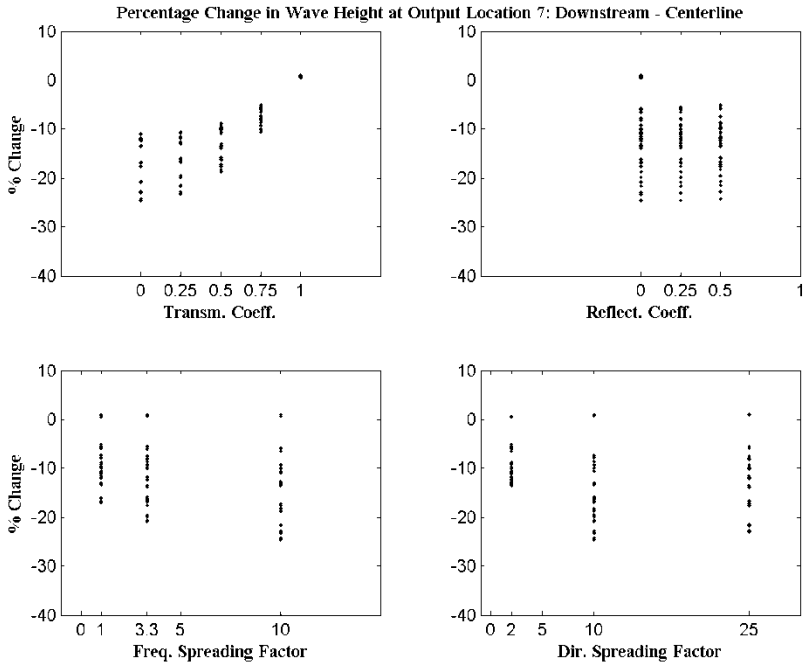


**Figure 22. Sensitivity analysis scatter plot for 10X to 2.5X spacing comparison at model output location 7: Downstream Centerline. The Y-axis is percent change in wave heights between 10X and 2.5X spacing.**

The distance effects of wave energy shadowing were evident upon comparison of these figures. A more closely spaced array blocked a larger amount of wave energy at the array location, which caused a larger decrease in wave height in the immediate lee of the array. The wave energy downstream dispersed rapidly, however, so far-field shadowing of wave height (e.g. greater than 5 km distant) was not observed. For larger spaced arrays, the wave energy may not have blocked as much in the near-field, but the effects propagated much further downstream: the wave field did not recover from the energy loss as rapidly.

Comparisons were made between all array spacing's evaluated in this study: 10X to 2.5X, 10X to 5X, and 5X to 2.5X. The largest differences in wave height are observed when comparing the 10X to 2.5X spacing. At output location 7, when the transmission coefficient is zero (most conservative), wave heights in the lee of the smaller spaced array are 10-25% smaller than those in the lee of the larger spaced array. The wave height decreases between 10X and 5X spacing at model output location 7 are not as large, varying between 10% and 20% for a transmission coefficient of 0. The wave height decrease between 5X and 2.5X is even smaller, varying between 0% and 10% for a transmission coefficient of 0. For comparison, at model output location 10, when the transmission coefficient is zero, wave heights in the lee of the smaller spaced array are up to 5% larger than those in the lee of the larger spaced array. This is a strong indication that the larger spaced array is still causing shadowing effects of the wave energy at this output location.

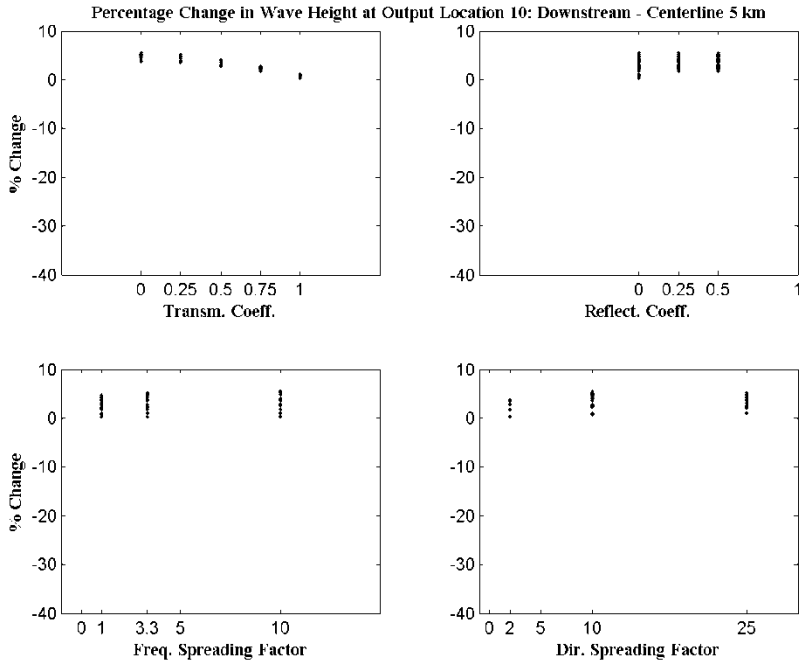


**Figure 23. Sensitivity analysis scatter plot for 10X to 2.5X spacing comparison at model output location 10: Downstream 5 km. The Y-axis is percent change in wave heights between 10X and 2.5X spacing.**

## 3.2. Diamond-Shaped WEC Array Simulation Results

Model results were retained for each model run listed in Appendix B (60 runs in total). Results included propagated wave heights, wave periods, wave directions, and near-bottom orbital velocities at all grid points in the model domains. Further, the same wave properties were extracted at each of the 18 distinct model output locations (Figure 15) to facilitate simple point-to-point comparison.

### *3.2.1. Significant Wave Height*

Figure 24, Figure 25, and Figure 26 show the results of significant wave height predictions from the sensitivity analysis. Images are surface-to-surface comparisons, comparing the modeled scenario results to the baseline scenario results. Black coloring indicates no (or negligible) change in wave height from the baseline scenario. Hotter colors indicate a larger amount of change (i.e. decrease in wave height) from the baseline scenario. Change is illustrated as a percentage change from the baseline scenario, computed as:

$$PercentageChange = \frac{(InitialValue - FinalValue)}{InitialValue} \times 100$$

In addition, the percentage change computed at each of the 18 model output locations is listed as text in each sub-figure, adjacent to the output location number; this allows for rapid comparison of the effect on significant wave heights from case to case.

In Figure 24, results from variable model transmission coefficients are shown. Here, the number of WEC devices was held constant at 50 and the WEC device array location was held constant at the 50 m depth contour. In Figure 25, the WEC array location was varied and the number of WEC devices was held constant at 50 and the transmission coefficient was held constant at 0.5. The number of WECs in the array was varied in Figure 26 while the transmission coefficient and depth of the WEC array were held constant at 0.5 and 50 m, respectively.

Immediately evident from examination of these figures was that the largest wave height decrease in lee of the WEC arrays occurred when the energy transmission was minimized (transmission coefficient is 0.3) and the number of WEC devices in an array was largest (i.e. 200 devices). Placement of the WEC array on the 40 m depth contour caused the largest nearshore wave height decreases along the Santa Cruz shoreline when compared to the 50 m or 60 m depth contour scenarios; however, it can be argued that placement at the 60 m depth contour, and, moreover, inclusion of a 200 WEC array, had the potential to disrupt a wider horizontal extent of significant wave heights (especially to the east of Santa Cruz, further east of the model output locations). Therefore, determination of a particular variable as the most sensitive variable in determining significant wave heights was difficult.

### *3.2.2. Near-bottom Orbital Velocity*

Near-bottom orbital velocities (e.g. wave-driven currents) were directly proportional to the surface wave expression (i.e. significant wave height). Decreased wave heights caused a decrease in near-bottom orbital velocities, potentially altering the ambient wave-driven currents in a nearshore environment. Consequently, the percentage differences of the near-bottom orbital velocities were essentially equivalent to those computed from the significant wave height model scenarios. Figures of near-bottom orbital velocity percentage differences were not included since they are equivalent to Figure 24, Figure 25, and Figure 26.

### *3.2.3. Peak Wave Period*

The percentage changes in peak wave periods during this study were negligible, as shown in Figure 27, Figure 28, and Figure 29. The reason for this was twofold. First, within the model parameters, the frequency bin resolution may have been too large to register small changes in wave periods (small changes in frequency would not have caused a change in frequency bin in model space). Second, since the model obstacles were “absorbing” the same percentage of wave energy from all wave frequencies (i.e. because the transmission coefficient was frequency-independent), there would have been no change in peak wave energy; the dominant wave energy would not shift to an alternate frequency(ies). Therefore, in the present study, no change (or negligible change) was observed.

### *3.2.4. Mean Wave Direction*

Changes in mean wave directions are illustrated in Figure 30, Figure 31, and Figure 32 as degrees changed (as opposed to percentage changes) for easy interpretation. Negative changes (blue) indicated clockwise (CW) rotation of wave direction. Positive changes (red) indicated counter-clockwise (CCW) rotation. Rotation, when it occurred, was relatively large, for the same reasons described for peak periods: the directional bin spacing was 15-degrees. Any changes less than this were indeterminable by the model.

Evident from the figures was that the mean wave directions were most affected by the largest WEC device array(s), which caused the largest horizontal extent wave shadowing effects in the lee of the array(s). As a result of transmission coefficient and depth contour variation, mean wave directions were altered, but changes were minor.

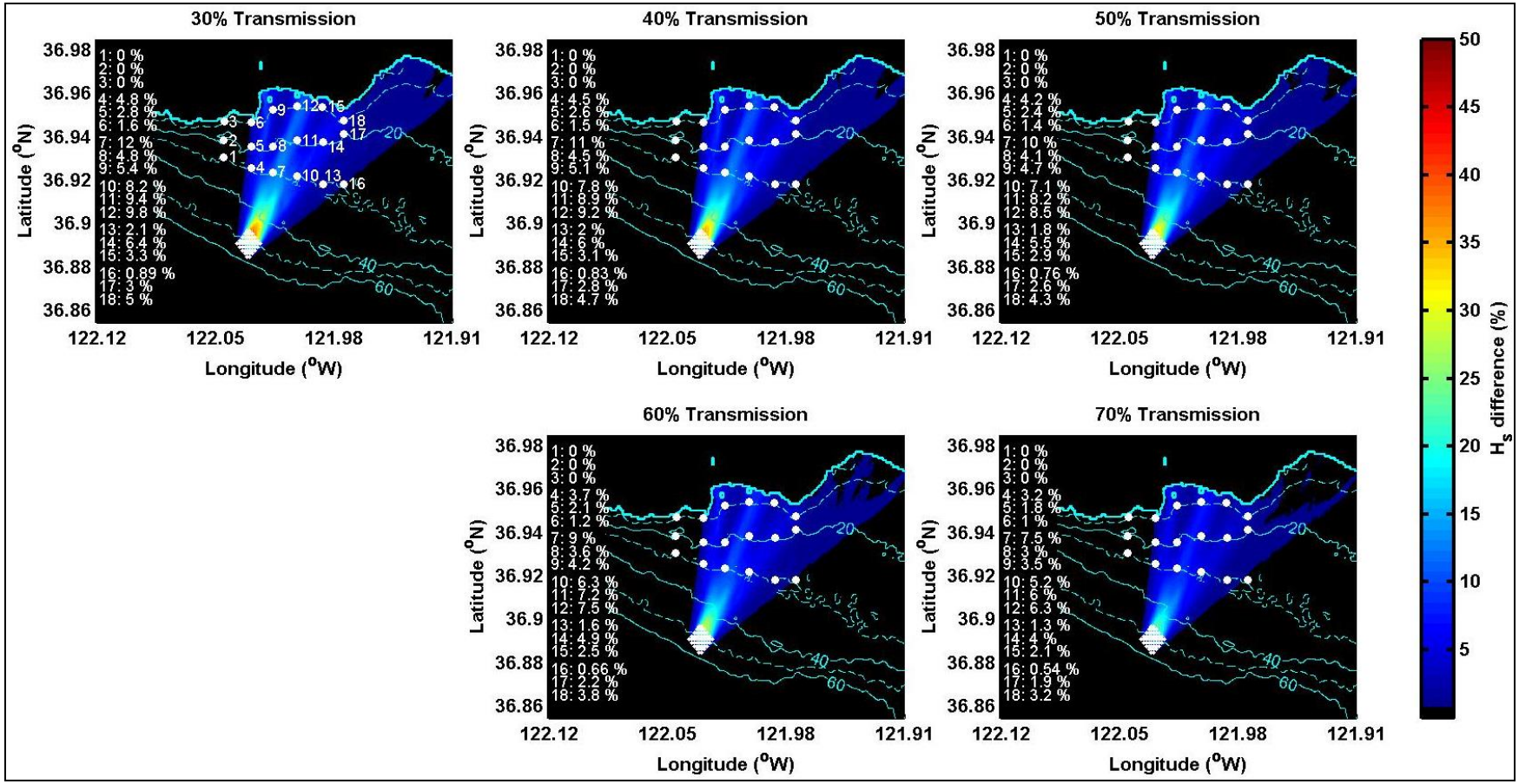


**Figure 24. Significant wave height percentage decrease as a result of varying transmission coefficient. The WEC device array was centered on the 50 m depth contour and comprised of 50 devices.**

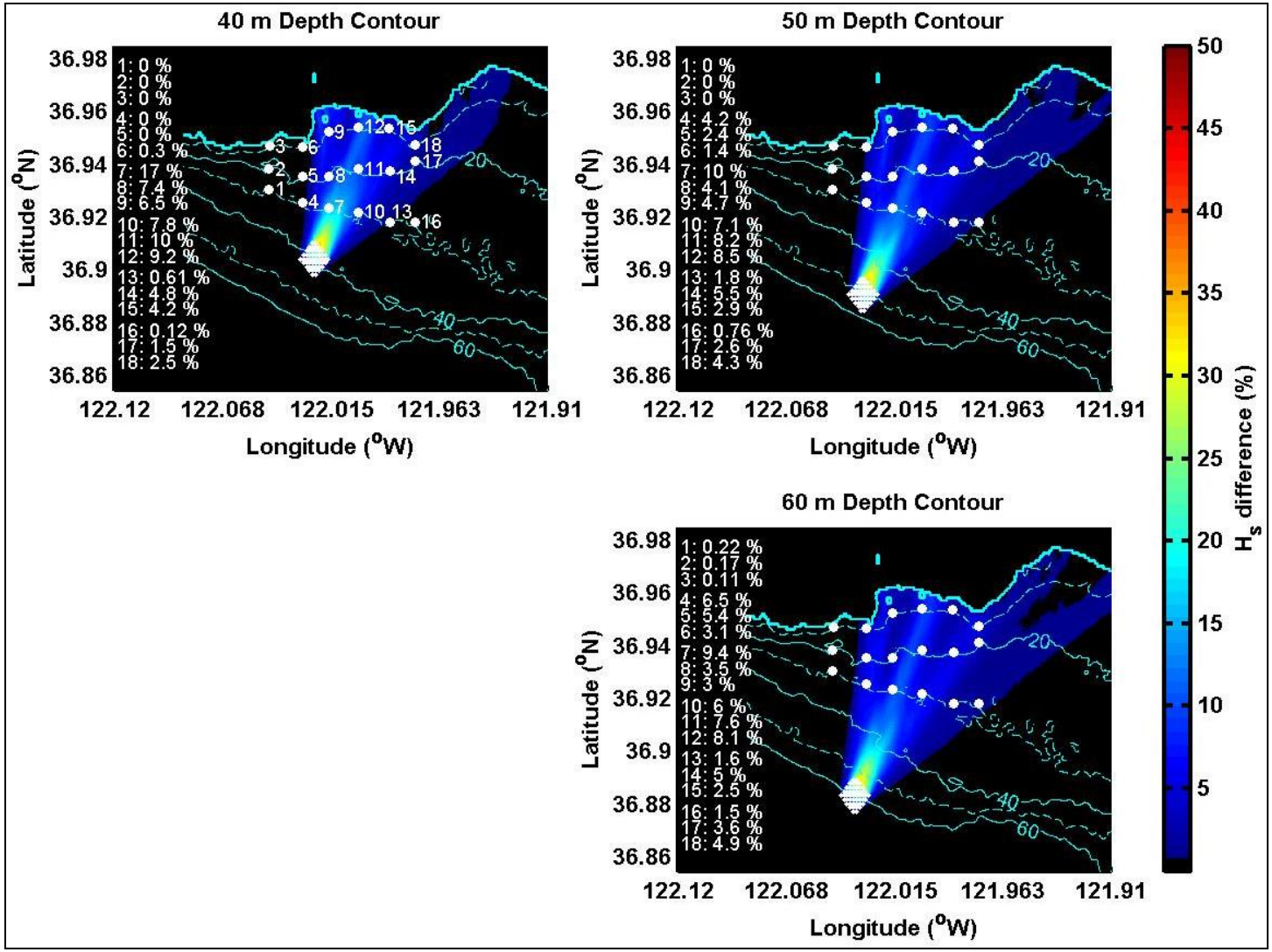


**Figure 25. Significant wave height percentage decrease as a result of varying depth contour location.**

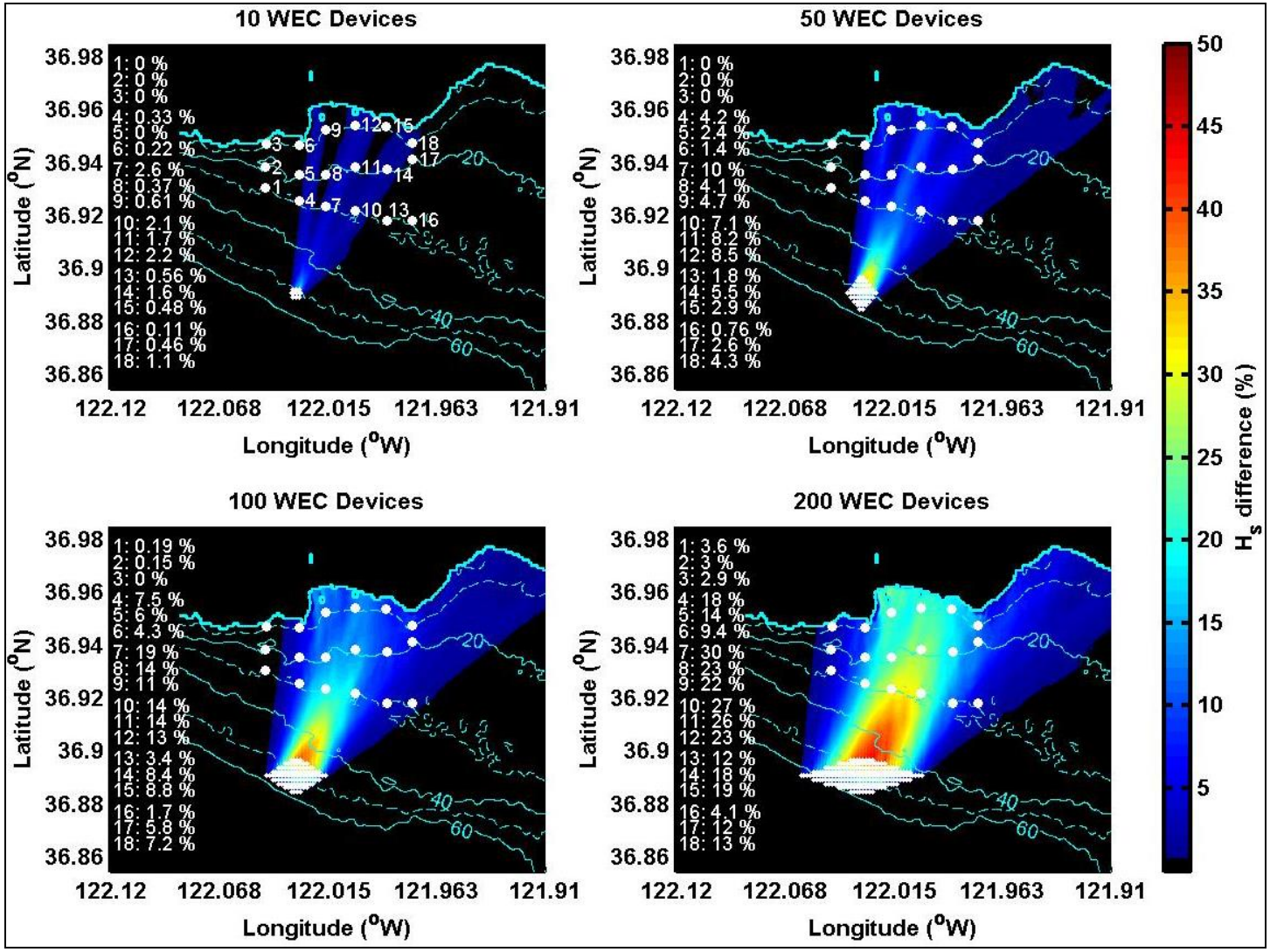


**Figure 26. Significant wave height percentage decrease as a result of varying number of WEC devices in the array.**

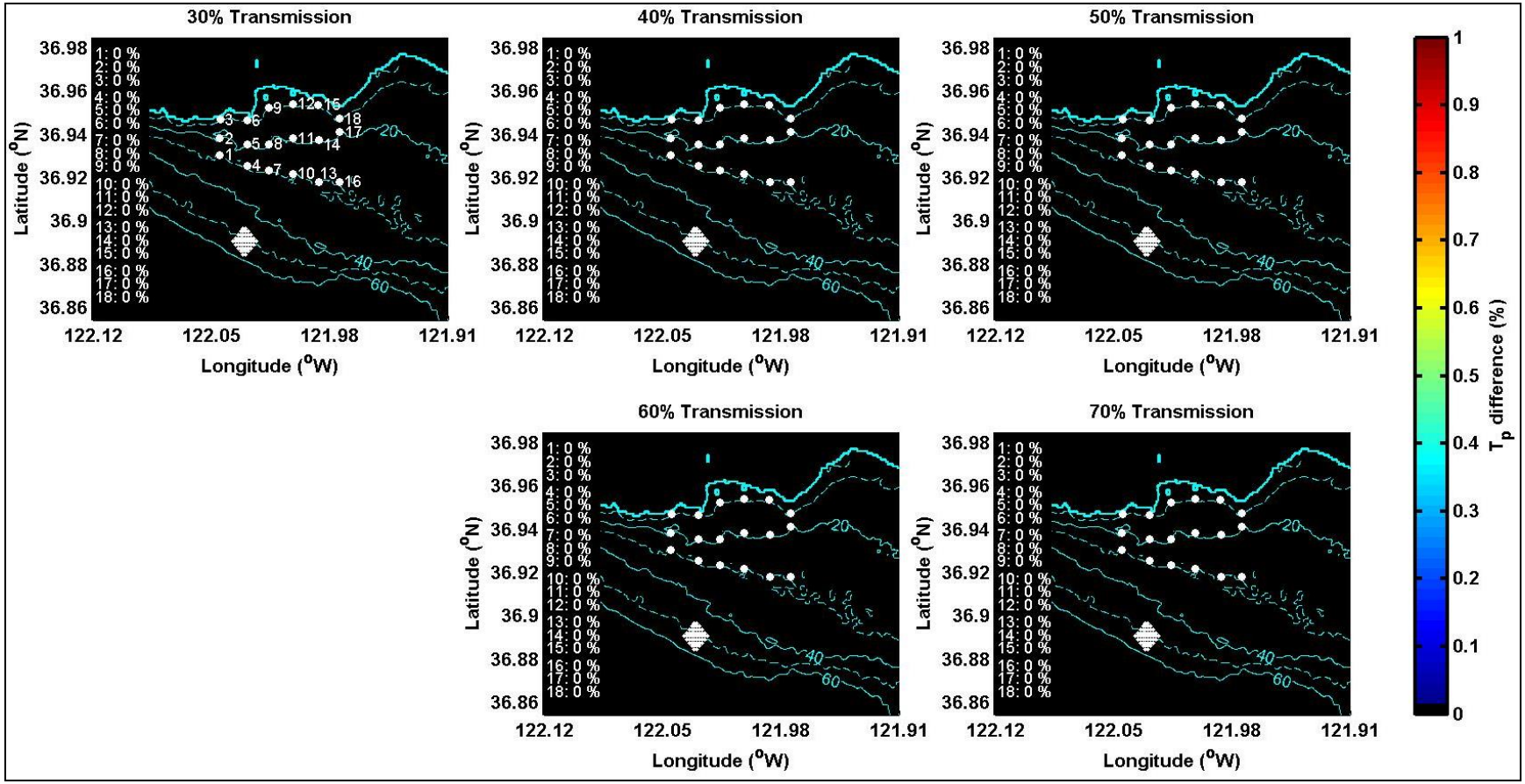


**Figure 27. Peak wave period percentage decrease as a result of varying transmission coefficient.**

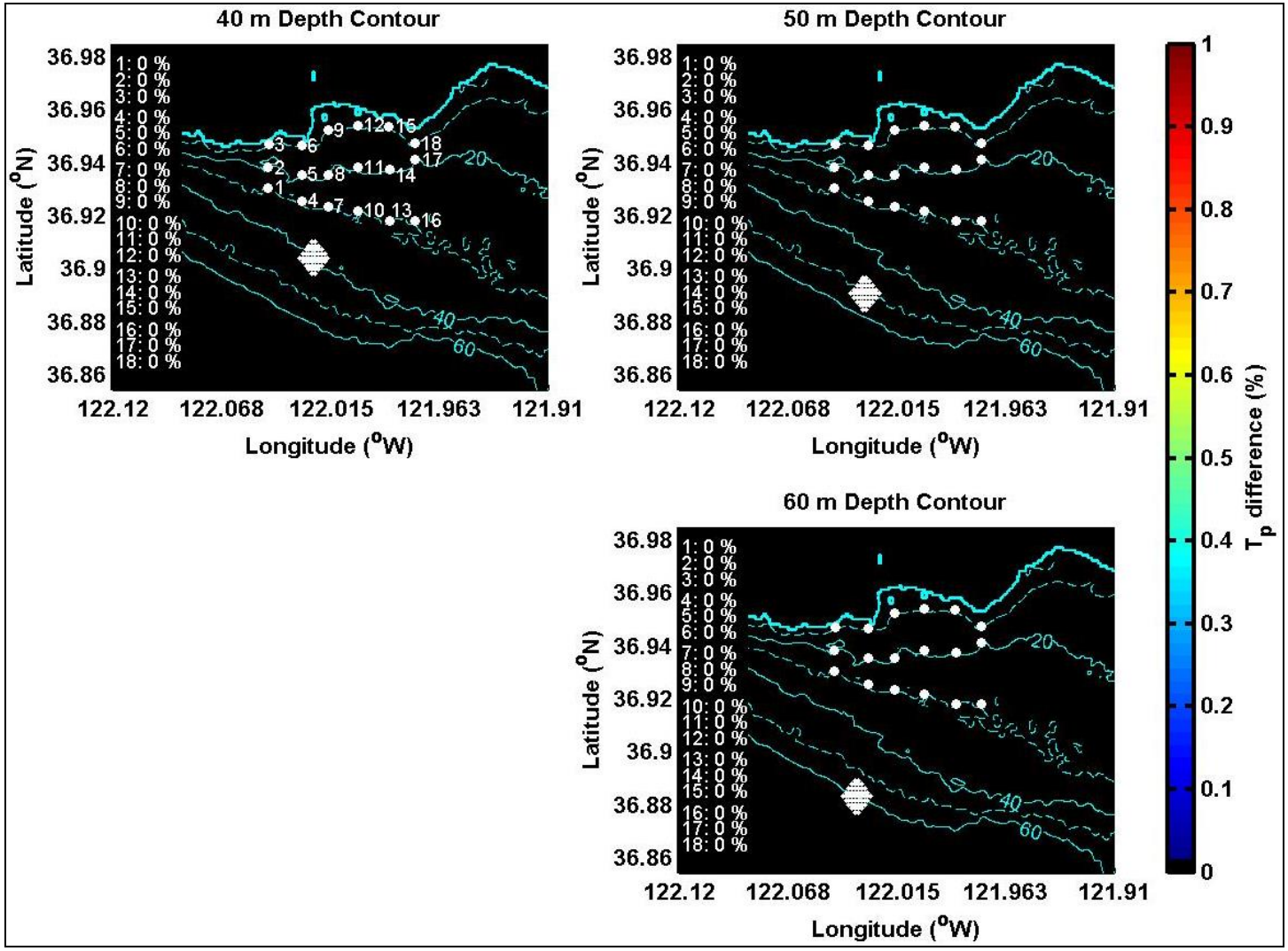


**Figure 28. Peak wave period percentage decrease as a result of varying depth contour location.**

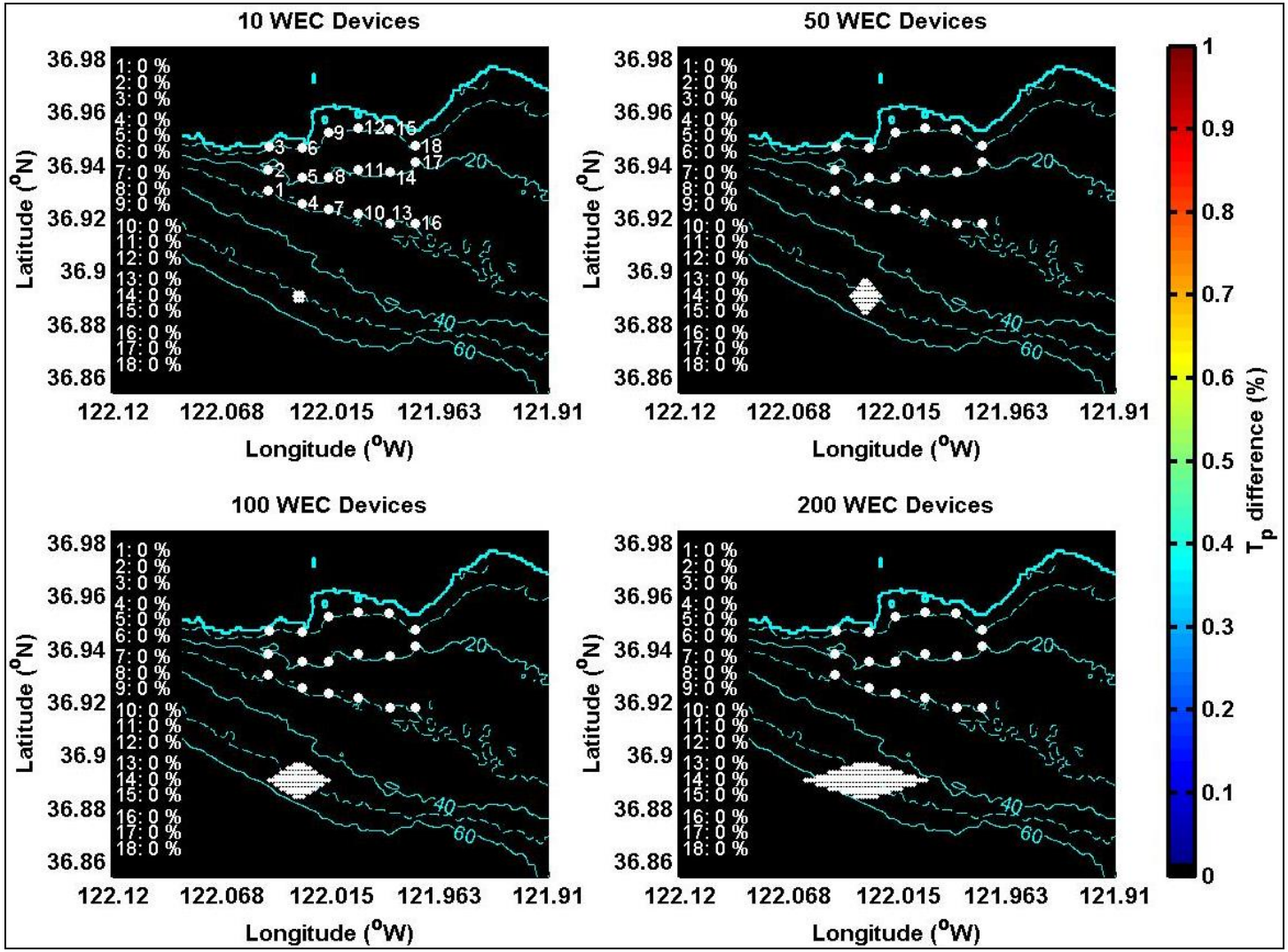


**Figure 29. Peak wave period percentage decrease as a result of varying number of WEC devices in the array.**

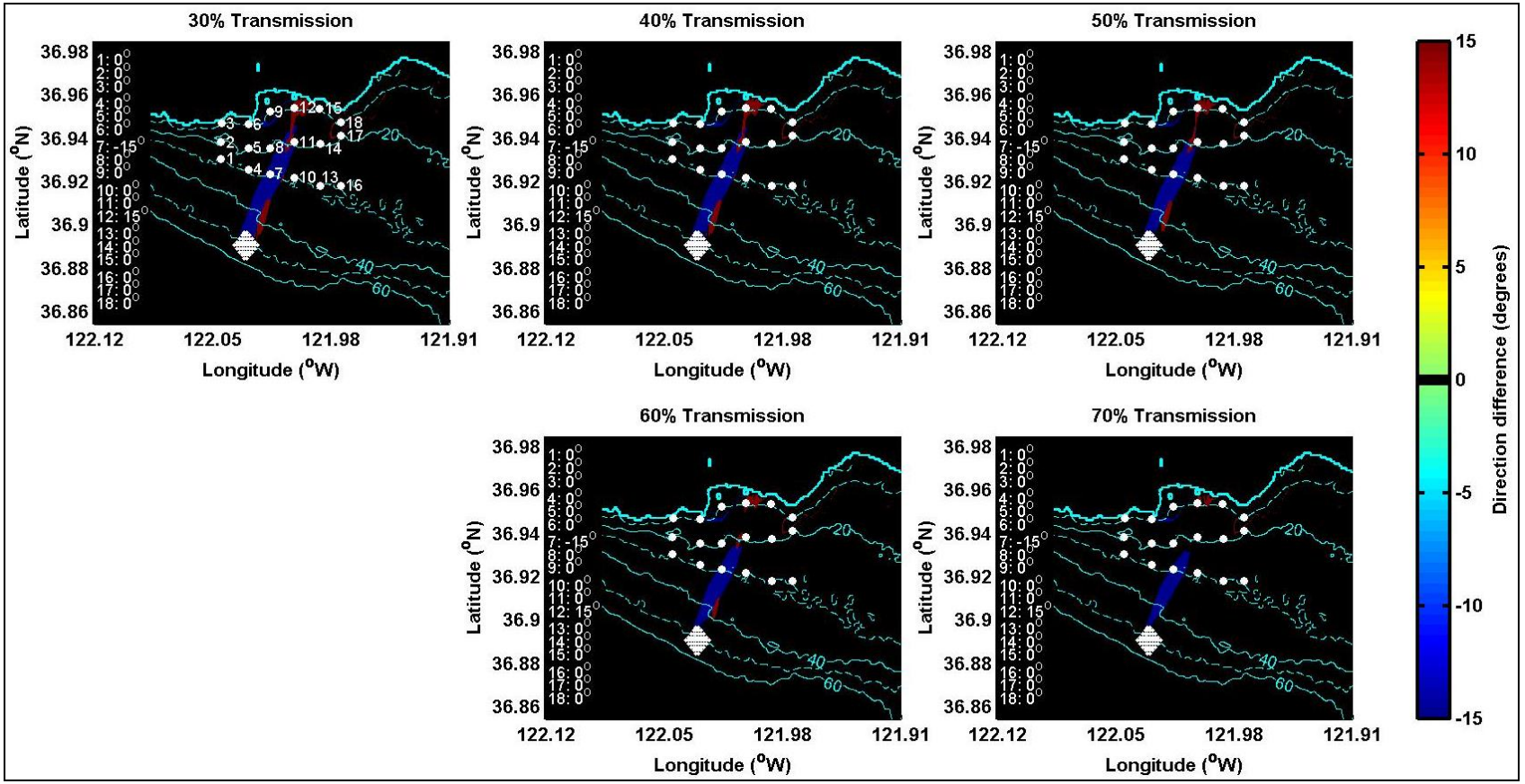


**Figure 30. Mean wave direction change (degrees) as a result of varying transmission coefficient.**

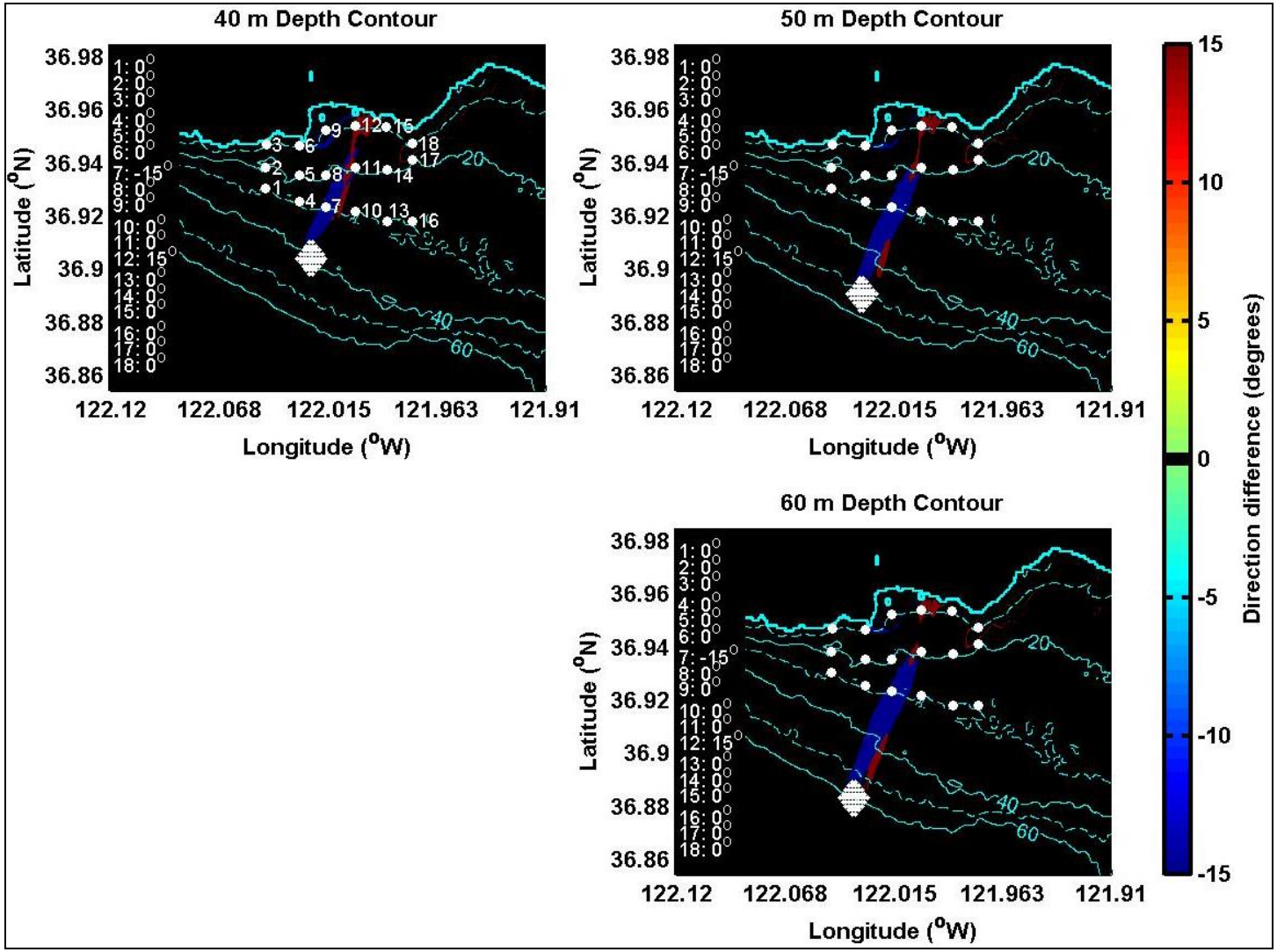


**Figure 31. Mean wave direction change (degrees) as a result of varying depth contour location.**

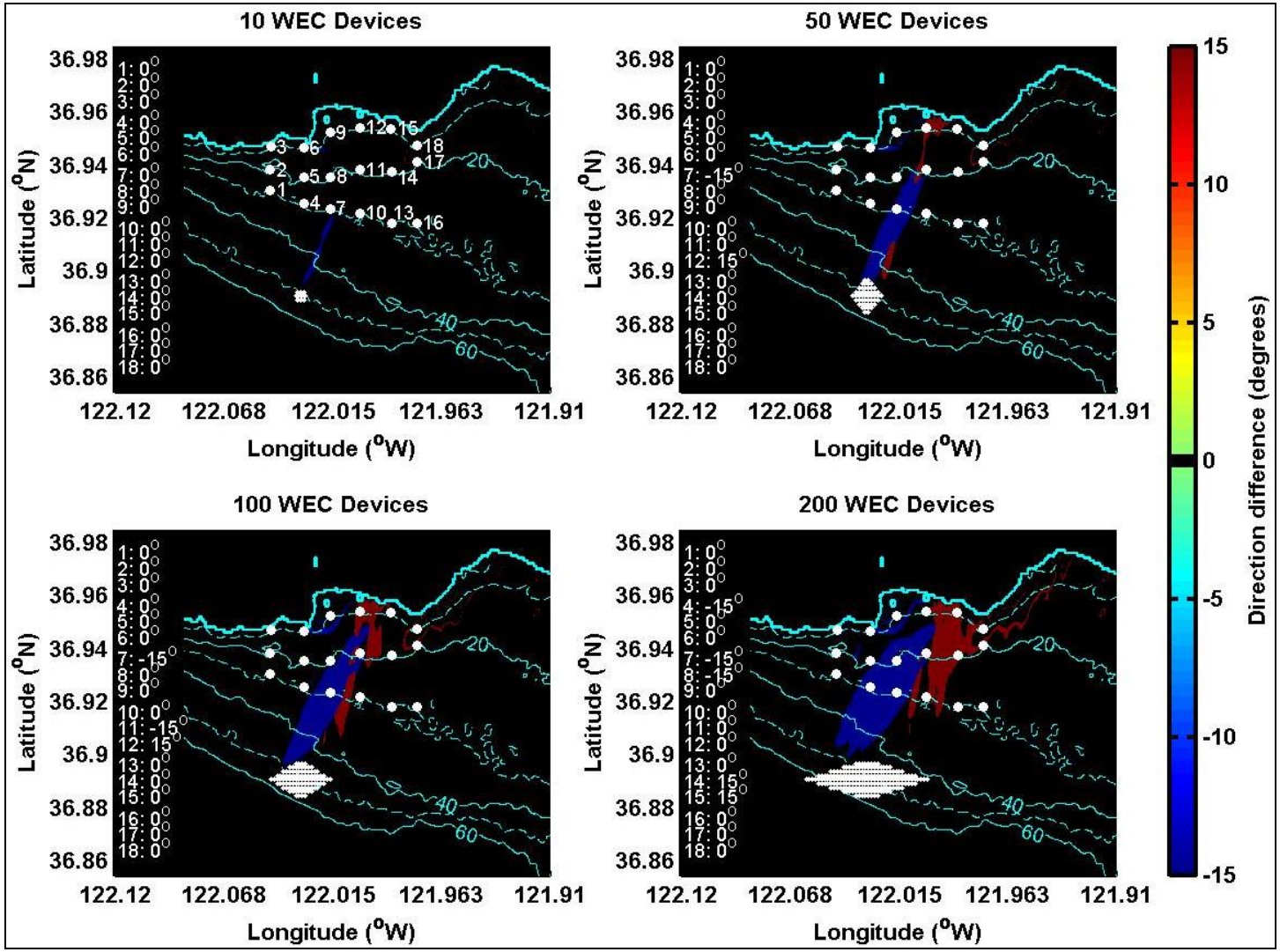


**Figure 32. Mean wave direction change (degrees) as a result of varying number of WEC devices in the array.**

### *3.2.5. Results Summary*

Figure 33 illustrates the total variation in all wave conditions versus transmission coefficient for all scenarios modeled in the present study. The shape of the scatter plots and degree of vertical spreading that existed for each constant parameter were indications of the model sensitivity to that parameter. For example, setting the transmission coefficient to 0.3 and allowing all other sensitivity parameters to vary resulted in a minimum wave height decrease of 0% (no change) and a maximum decrease in wave height of ~42% over all scenarios modeled (top left subplot, Figure 33).

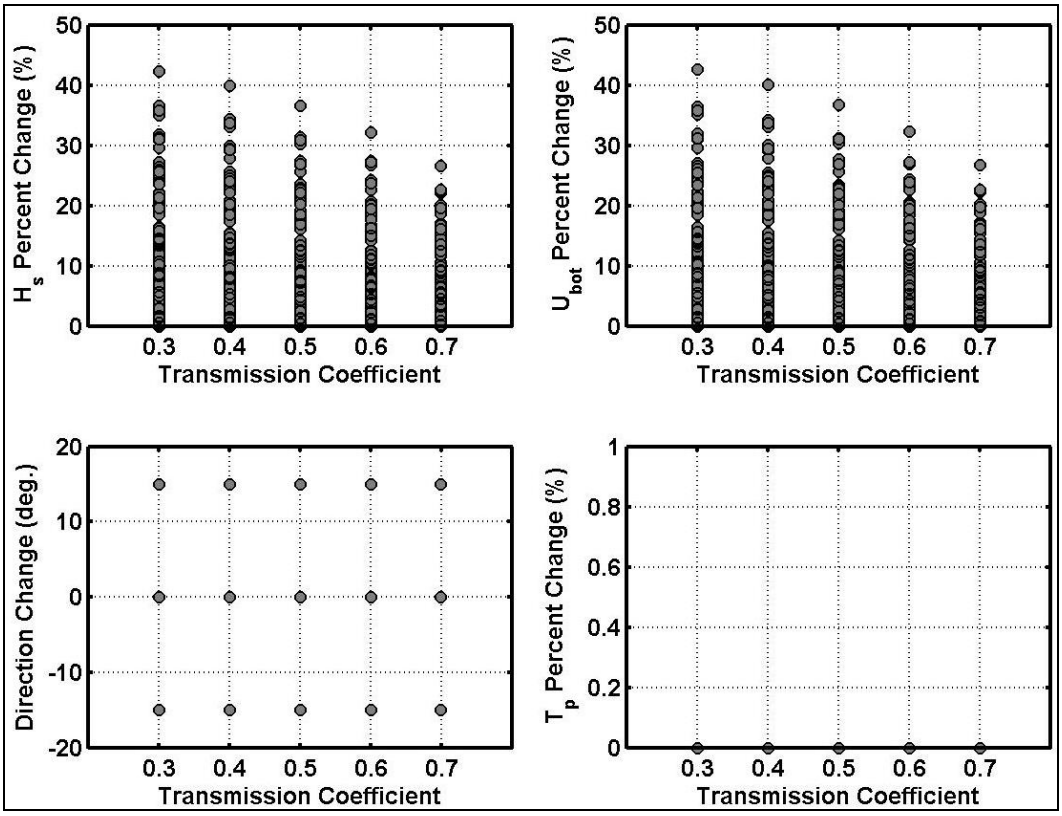


**Figure 33. Variation in wave properties versus transmission coefficients.**

Figure 33 illustrates that both wave height and near-bottom orbital velocity were subject to the largest potential variations, each decreasing in sensitivity as transmission coefficient increased. Wave direction was affected consistently for all transmission coefficients; and wave period was not affected (or negligibly affected) by varying transmission coefficient. Similar results were observed in Figure 34 and Figure 35, which indicate the range of changes anticipated by varying the depth contour and number of WEC devices in the array, respectively. Wave heights and near-bottom orbital velocities showed the greatest amount of variation nearer to shore (40 m depth contour) and as the number of WEC devices in the array increased (200 device array).

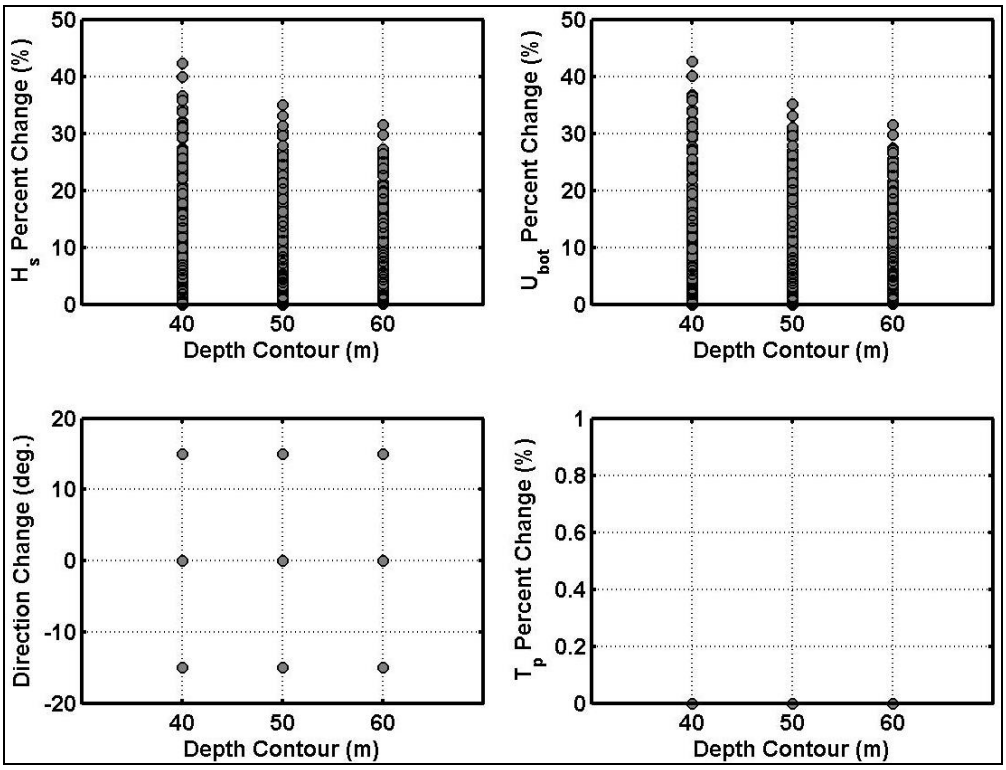


**Figure 34. Variation in wave properties versus depth contours.**

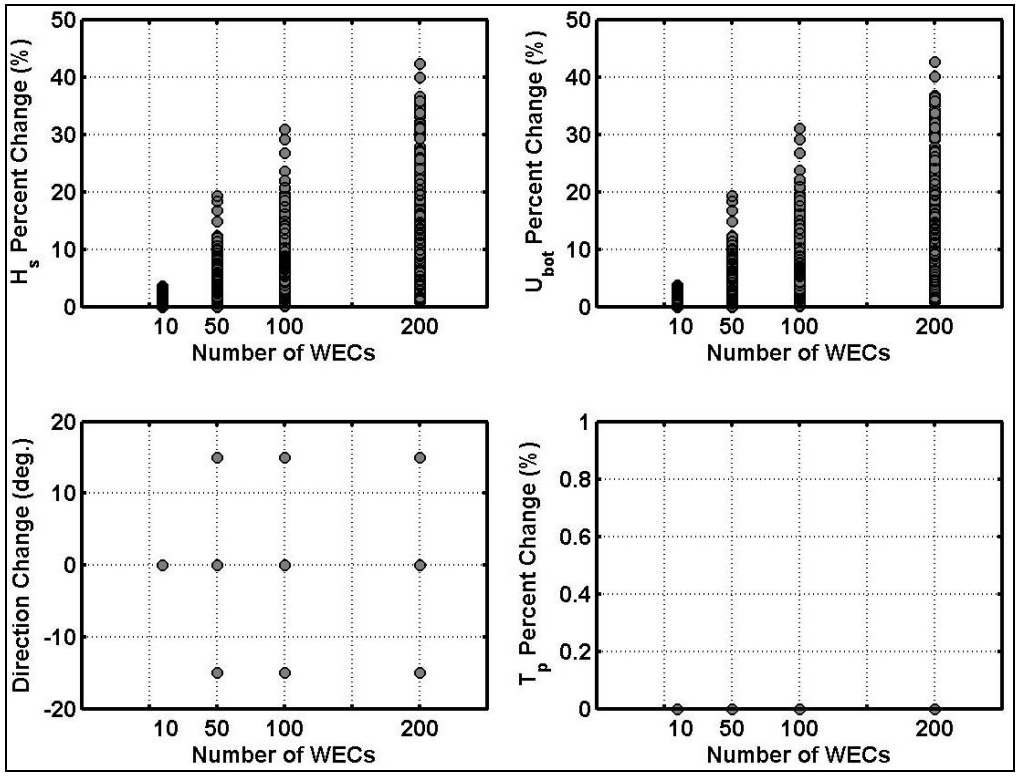


**Figure 35. Variation in wave properties versus number of WEC devices in the array.**

Another means with which to view the model results is presented in Figure 36 through Figure 38, which allow determination of the model parameters that have the greatest effect on the specific wave properties. From Figure 36 it is evident that the largest wave height variation was expected when the transmission coefficient was lowest (0.3), the deployment location was the shallowest (40 m depth contour), and the number of WEC devices in the array was the largest (200 devices). This scenario corresponded to the most wave energy "absorption", shallowest array location and largest horizontal extent "disruption" of wave energy propagation (due to the large number of obstacles).

The peak wave periods were not affected (or are negligibly affected) by variation of the parameters (Figure 37). The mean wave direction variation was minimized for the smallest number of WEC devices in the array (10 WEC devices, top left subplot); but remained constant for all other parameter variations (Figure 38).

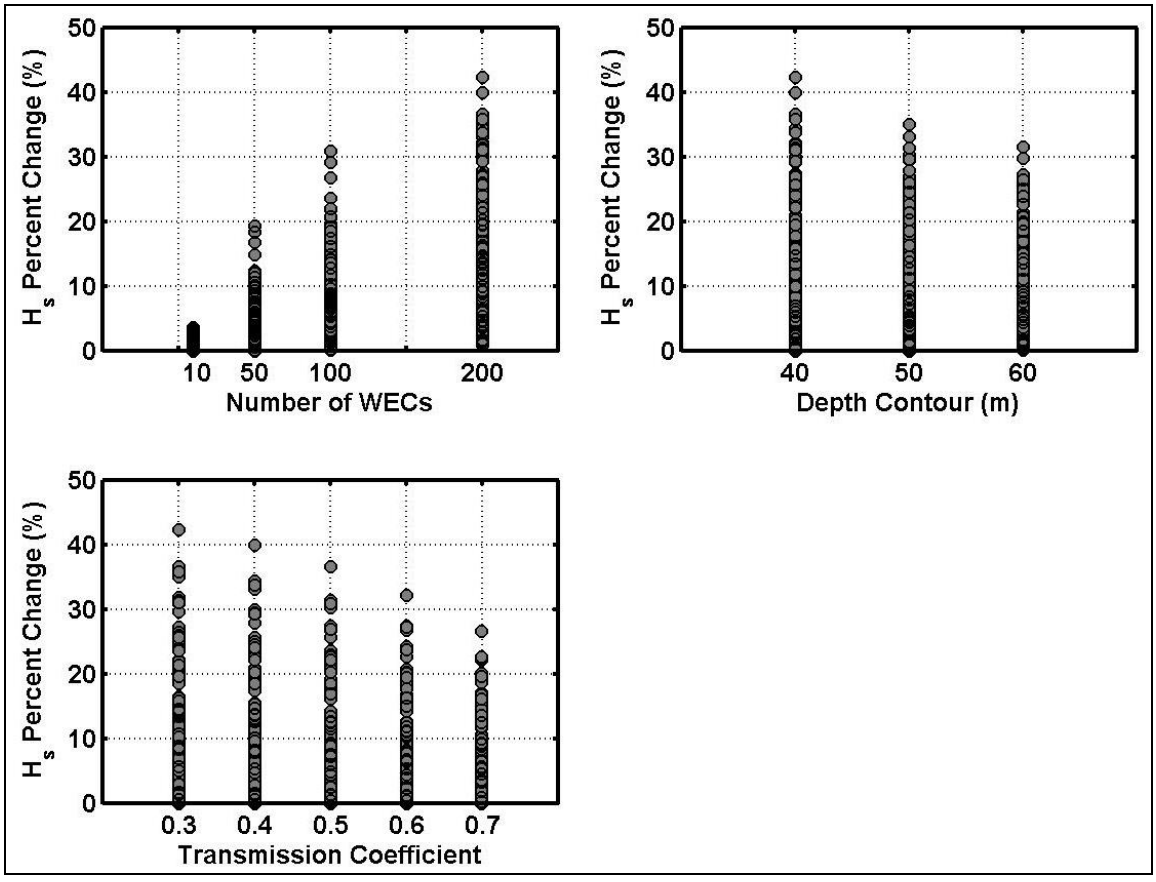


**Figure 36. Variation in significant wave height for all varied parameters.**

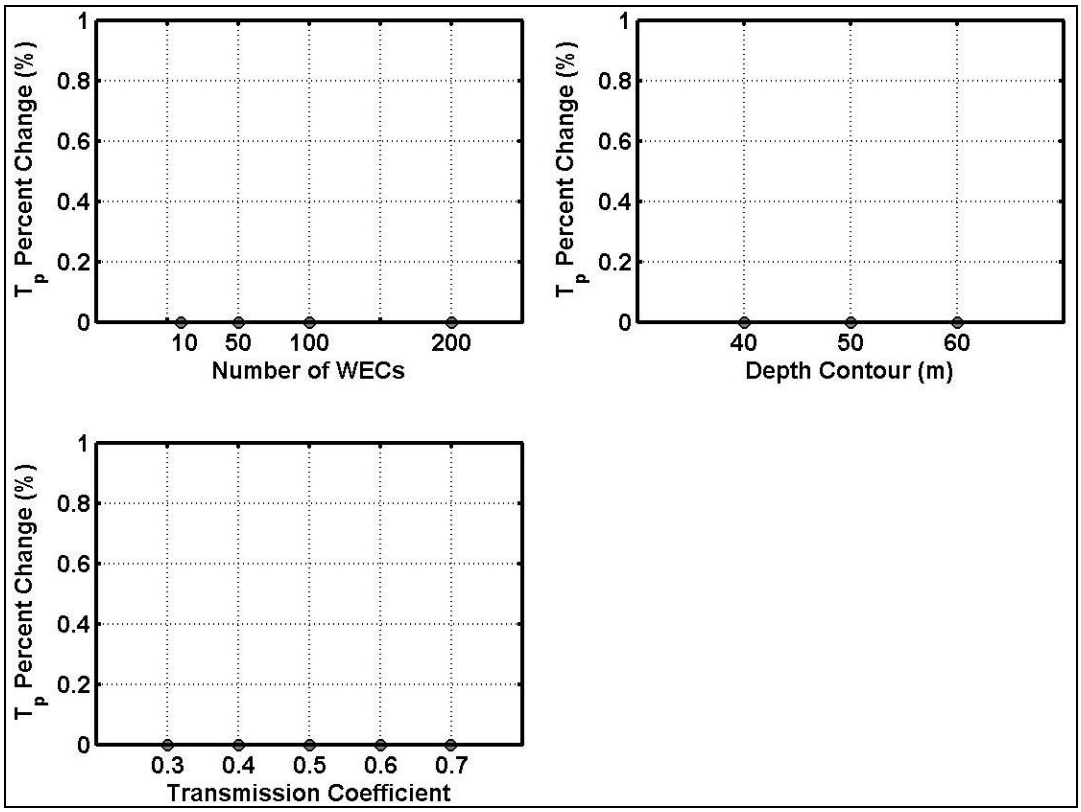


**Figure 37. Variation in peak wave period for all varied parameters.**

These results ultimately illustrated, that, given the present model setup, the wave heights (and associated near-bottom orbital velocities) were most sensitive to the selected variables. Wave periods did not appear to be sensitive to changes in parameters; moreover, wave direction was not as sensitive to changes in the parameters, but did show some variation. However, additional analysis is required to fully explore the model sensitivity of peak wave period and mean wave direction to the varying of the parameters.

Model output locations to the East and West of the array showed relatively little to no change in wave heights compared to the baseline scenario. The largest wave height differences were observed downstream of the array near the array centerline (output locations 7 through 12), where the largest wave shadowing effects were predicted. Depending upon the parameters selected during each scenario, additional model output locations may also have indicated large changes in wave heights (e.g. output locations such as 14 and 15, which were more affected by a large WEC array).

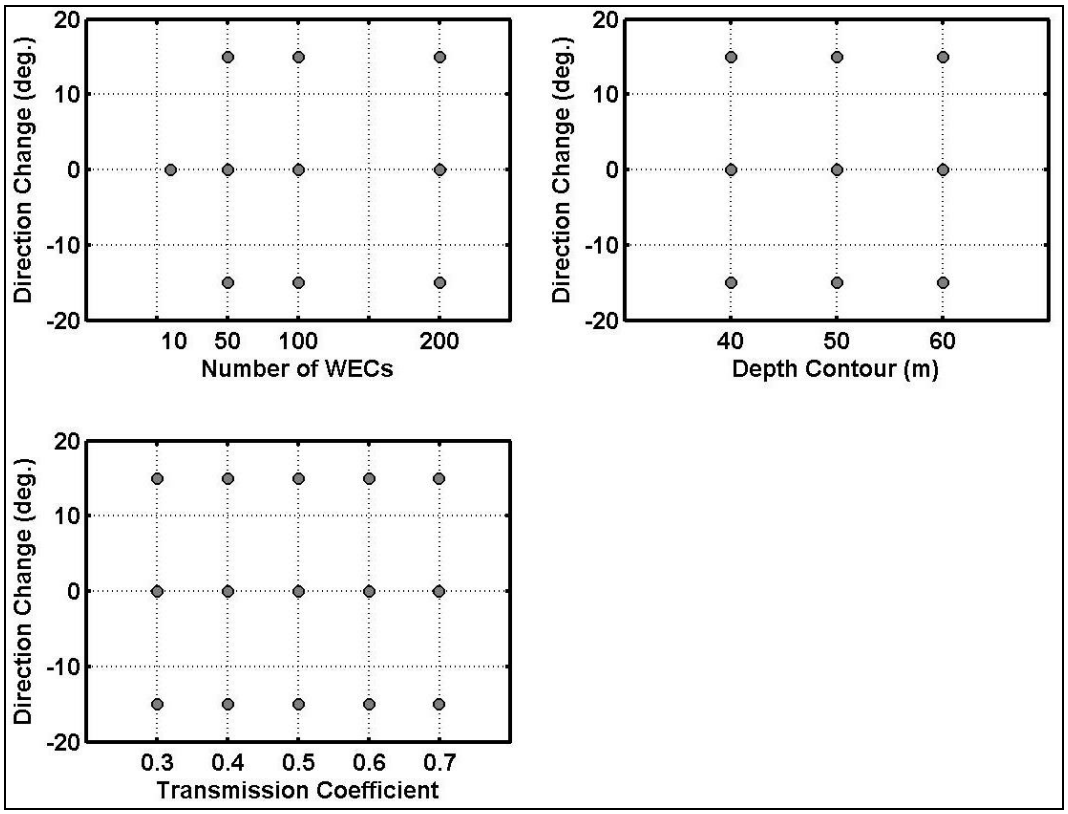


**Figure 38. Variation in mean wave direction for all varied parameters.**

# 4. CONCLUSIONS

The presence of WEC arrays have the potential to alter wave propagation patterns significantly and affect coastal circulation, sediment transport patterns, and alter ecosystem processes. Since no commercial-scale arrays have been installed at a real world site yet, we must rely on predictive modeling tools to investigate the ranges of anticipated scenarios and evaluate the potential for environmental impact. Here, an industry standard wave modeling tool, SWAN, was utilized to examine a proposed wave array deployment at a site on the California coast. Two different types of simulations were used to investigate model sensitivity (honeycomb and diamond-shaped) so that the model can be effectively and confidently used in environmental studies.

The honeycomb WEC array sensitivity study illustrated that wave heights were most sensitive to the transmission coefficient and that the other model parameters had a minimal effect on overall change in wave height. Similar evaluations were made for the wave period and wave direction sensitivity to model parameters. In general, wave period decreases were also sensitive to the transmission coefficient, and, to a lesser degree, the directional spreading factor (lower directional spreading coefficient resulted in less scatter in model prediction). Wave direction was not as sensitive to changes in the coefficients as the other wave parameters (changes were small or negligible between baseline and array scenarios). Some changes were observed; however, additional analysis is required to fully explain the model sensitivity of mean wave direction to the varying of the parameters.

Results from the honeycomb WEC array study suggested that array device spacing had an effect on downstream wave conditions, both near-field and far-field. Based on visual observation, closer spacing of WEC devices (e.g. 2.5X) resulted in a larger decrease in wave energy propagation near the array compared to larger spaced arrays (5X or 10X spacing). The far-field effect of a closer-spaced array on the wave conditions was not as significant as larger-spaced arrays.

Generally, the changes in wave height were the primary alteration resulting in the presence of a WEC array. The spacing of an array had a significant effect on downstream wave properties. It appeared that reasonable ranges of directional spreading coefficients had minimal effects on the overall results. The transmission coefficient was shown to generate the largest sensitivity in honeycomb WEC array simulations; therefore model obstacle transmission coefficients were further investigated in conjunction with the number of WEC devices (obstacles) specified in a diamond-shaped WEC array, and the diamond-shaped array deployment location (depth contour).

The diamond-shaped WEC array sensitivity study illustrated that the wave heights were most sensitive to the variation in the parameters examined in this study. Locations in the lee centerline of the arrays in each modeled scenario showed the largest potential changes in wave height (and near-bottom orbital velocity) compared to those at the eastern and western fringes of the shadow zone. The largest wave height variation was realized when the transmission coefficient was lowest (0.3), the deployment location was the shallowest (40 m depth contour) and closest to shore, and the number of WEC devices in the array was the largest (200 devices). This scenario

corresponded to the most wave energy "absorption", shallowest array location and largest horizontal extent "disruption" of wave energy propagation (due to the large number of obstacles).

Both wave height and near-bottom orbital velocity were subject to the largest potential variations, each decreasing in sensitivity as transmission coefficient increased, as number of WEC devices decreased, and as the deployment location moved offshore. Wave direction was affected consistently for all parameters; and wave period was not affected (or negligibly affected) by varying parameters.

Generally, the changes in wave height were the primary alteration caused by the presence of a WEC array. Specifically, transmission coefficient variations directly resulted in wave height variations; however, it is important to utilize ongoing laboratory studies and future field tests to determine the most appropriate transmission coefficient values for a particular WEC device and configuration. Until transmission coefficient values can be accurately determined or WEC 'friendly' model enhancements are validated, this study showed that environmental assessments of WEC devices should focus on evaluating a range of transmission coefficients in order to determine the potential effects resulting from the presence of a WEC array.

The study results also indicated that further sensitivity analysis may be required to refine the model predictions and interpretations. Specifically,

- The frequency and directional bin spacing settings in the model should be minimized to more effectively evaluate the small-scale changes in wave period and direction resulting from WEC arrays.
- Frequency and directional spreading parameter variation, and their impact on downstream wave shadowing should be investigated further to determine the appropriate leeward distance at which a wave field "recovers" from the shadowing effects of WEC arrays.
- Multiple offshore incident wave angles should be examined to determine the likelihood of WEC array effects reaching shorelines.

# 5. REFERENCES


1. Booij, N., Holthuijsen, L.H. and R.C. Ris, 1996, The SWAN wave model for shallow water, Proc. 25th Int. Conf. Coastal Engng., Orlando, USA, Vol. 1, pp. 668-676.

2. Chang, G and C. Jones, D. Hansen, M. Twardowski and A. Barnard, 2010, Prediction of Optical Variability in Dynamic Near-shore Environments: Task Completion Report #3 – Numerical Modeling and Verification. 28 pp.

# APPENDIX A: HONEYCOMB WEC ARRAY MODEL SENSITIVITY PARAMETERS

| Run | Input $H_s$ (m) | Input $T_p$ (s) | Input MWD (deg) | Transm Coeff | Reflect Coeff | Gamma – Freq Spreading | M – Dir Spreading |
|---|---|---|---|---|---|---|---|
| 1 | 2 | 12 | 310 | 0.00 | 0.00 | 1.00 | 2.00 |
| 2 | 2 | 12 | 310 | 0.00 | 0.00 | 1.00 | 10.00 |
| 3 | 2 | 12 | 310 | 0.00 | 0.00 | 1.00 | 25.00 |
| 4 | 2 | 12 | 310 | 0.00 | 0.00 | 3.30 | 2.00 |
| 5 | 2 | 12 | 310 | 0.00 | 0.00 | 3.30 | 10.00 |
| 6 | 2 | 12 | 310 | 0.00 | 0.00 | 3.30 | 25.00 |
| 7 | 2 | 12 | 310 | 0.00 | 0.00 | 10.00 | 2.00 |
| 8 | 2 | 12 | 310 | 0.00 | 0.00 | 10.00 | 10.00 |
| 9 | 2 | 12 | 310 | 0.00 | 0.00 | 10.00 | 25.00 |
| 10 | 2 | 12 | 310 | 0.00 | 0.25 | 1.00 | 2.00 |
| 11 | 2 | 12 | 310 | 0.00 | 0.25 | 1.00 | 10.00 |
| 12 | 2 | 12 | 310 | 0.00 | 0.25 | 1.00 | 25.00 |
| 13 | 2 | 12 | 310 | 0.00 | 0.25 | 3.30 | 2.00 |
| 14 | 2 | 12 | 310 | 0.00 | 0.25 | 3.30 | 10.00 |
| 15 | 2 | 12 | 310 | 0.00 | 0.25 | 3.30 | 25.00 |
| 16 | 2 | 12 | 310 | 0.00 | 0.25 | 10.00 | 2.00 |
| 17 | 2 | 12 | 310 | 0.00 | 0.25 | 10.00 | 10.00 |
| 18 | 2 | 12 | 310 | 0.00 | 0.25 | 10.00 | 25.00 |
| 19 | 2 | 12 | 310 | 0.00 | 0.50 | 1.00 | 2.00 |
| 20 | 2 | 12 | 310 | 0.00 | 0.50 | 1.00 | 10.00 |
| 21 | 2 | 12 | 310 | 0.00 | 0.50 | 1.00 | 25.00 |
| 22 | 2 | 12 | 310 | 0.00 | 0.50 | 3.30 | 2.00 |
| 23 | 2 | 12 | 310 | 0.00 | 0.50 | 3.30 | 10.00 |
| 24 | 2 | 12 | 310 | 0.00 | 0.50 | 3.30 | 25.00 |
| 25 | 2 | 12 | 310 | 0.00 | 0.50 | 10.00 | 2.00 |
| 26 | 2 | 12 | 310 | 0.00 | 0.50 | 10.00 | 10.00 |
| 27 | 2 | 12 | 310 | 0.00 | 0.50 | 10.00 | 25.00 |
| 28 | 2 | 12 | 310 | 0.25 | 0.00 | 1.00 | 2.00 |
| 29 | 2 | 12 | 310 | 0.25 | 0.00 | 1.00 | 10.00 |
| 30 | 2 | 12 | 310 | 0.25 | 0.00 | 1.00 | 25.00 |
| 31 | 2 | 12 | 310 | 0.25 | 0.00 | 3.30 | 2.00 |
| 32 | 2 | 12 | 310 | 0.25 | 0.00 | 3.30 | 10.00 |
| 33 | 2 | 12 | 310 | 0.25 | 0.00 | 3.30 | 25.00 |
| 34 | 2 | 12 | 310 | 0.25 | 0.00 | 10.00 | 2.00 |
| 35 | 2 | 12 | 310 | 0.25 | 0.00 | 10.00 | 10.00 |
| 36 | 2 | 12 | 310 | 0.25 | 0.00 | 10.00 | 25.00 |
| 37 | 2 | 12 | 310 | 0.25 | 0.25 | 1.00 | 2.00 |
| 38 | 2 | 12 | 310 | 0.25 | 0.25 | 1.00 | 10.00 |
| 39 | 2 | 12 | 310 | 0.25 | 0.25 | 1.00 | 25.00 |
| 40 | 2 | 12 | 310 | 0.25 | 0.25 | 3.30 | 2.00 |
| 41 | 2 | 12 | 310 | 0.25 | 0.25 | 3.30 | 10.00 |

| | | | | | | | |
|---|---|---|---|---|---|---|---|
| 42 | 2 | 12 | 310 | 0.25 | 0.25 | 3.30 | 25.00 |
| 43 | 2 | 12 | 310 | 0.25 | 0.25 | 10.00 | 2.00 |
| 44 | 2 | 12 | 310 | 0.25 | 0.25 | 10.00 | 10.00 |
| 45 | 2 | 12 | 310 | 0.25 | 0.25 | 10.00 | 25.00 |
| 46 | 2 | 12 | 310 | 0.25 | 0.50 | 1.00 | 2.00 |
| 47 | 2 | 12 | 310 | 0.25 | 0.50 | 1.00 | 10.00 |
| 48 | 2 | 12 | 310 | 0.25 | 0.50 | 1.00 | 25.00 |
| 49 | 2 | 12 | 310 | 0.25 | 0.50 | 3.30 | 2.00 |
| 50 | 2 | 12 | 310 | 0.25 | 0.50 | 3.30 | 10.00 |
| 51 | 2 | 12 | 310 | 0.25 | 0.50 | 3.30 | 25.00 |
| 52 | 2 | 12 | 310 | 0.25 | 0.50 | 10.00 | 2.00 |
| 53 | 2 | 12 | 310 | 0.25 | 0.50 | 10.00 | 10.00 |
| 54 | 2 | 12 | 310 | 0.25 | 0.50 | 10.00 | 25.00 |
| 55 | 2 | 12 | 310 | 0.50 | 0.00 | 1.00 | 2.00 |
| 56 | 2 | 12 | 310 | 0.50 | 0.00 | 1.00 | 10.00 |
| 57 | 2 | 12 | 310 | 0.50 | 0.00 | 1.00 | 25.00 |
| 58 | 2 | 12 | 310 | 0.50 | 0.00 | 3.30 | 2.00 |
| 59 | 2 | 12 | 310 | 0.50 | 0.00 | 3.30 | 10.00 |
| 60 | 2 | 12 | 310 | 0.50 | 0.00 | 3.30 | 25.00 |
| 61 | 2 | 12 | 310 | 0.50 | 0.00 | 10.00 | 2.00 |
| 62 | 2 | 12 | 310 | 0.50 | 0.00 | 10.00 | 10.00 |
| 63 | 2 | 12 | 310 | 0.50 | 0.00 | 10.00 | 25.00 |
| 64 | 2 | 12 | 310 | 0.50 | 0.25 | 1.00 | 2.00 |
| 65 | 2 | 12 | 310 | 0.50 | 0.25 | 1.00 | 10.00 |
| 66 | 2 | 12 | 310 | 0.50 | 0.25 | 1.00 | 25.00 |
| 67 | 2 | 12 | 310 | 0.50 | 0.25 | 3.30 | 2.00 |
| 68 | 2 | 12 | 310 | 0.50 | 0.25 | 3.30 | 10.00 |
| 69 | 2 | 12 | 310 | 0.50 | 0.25 | 3.30 | 25.00 |
| 70 | 2 | 12 | 310 | 0.50 | 0.25 | 10.00 | 2.00 |
| 71 | 2 | 12 | 310 | 0.50 | 0.25 | 10.00 | 10.00 |
| 72 | 2 | 12 | 310 | 0.50 | 0.25 | 10.00 | 25.00 |
| 73 | 2 | 12 | 310 | 0.50 | 0.50 | 1.00 | 2.00 |
| 74 | 2 | 12 | 310 | 0.50 | 0.50 | 1.00 | 10.00 |
| 75 | 2 | 12 | 310 | 0.50 | 0.50 | 1.00 | 25.00 |
| 76 | 2 | 12 | 310 | 0.50 | 0.50 | 3.30 | 2.00 |
| 77 | 2 | 12 | 310 | 0.50 | 0.50 | 3.30 | 10.00 |
| 78 | 2 | 12 | 310 | 0.50 | 0.50 | 3.30 | 25.00 |
| 79 | 2 | 12 | 310 | 0.50 | 0.50 | 10.00 | 2.00 |
| 80 | 2 | 12 | 310 | 0.50 | 0.50 | 10.00 | 10.00 |
| 81 | 2 | 12 | 310 | 0.50 | 0.50 | 10.00 | 25.00 |
| 82 | 2 | 12 | 310 | 0.75 | 0.00 | 1.00 | 2.00 |
| 83 | 2 | 12 | 310 | 0.75 | 0.00 | 1.00 | 10.00 |
| 84 | 2 | 12 | 310 | 0.75 | 0.00 | 1.00 | 25.00 |
| 85 | 2 | 12 | 310 | 0.75 | 0.00 | 3.30 | 2.00 |
| 86 | 2 | 12 | 310 | 0.75 | 0.00 | 3.30 | 10.00 |
| 87 | 2 | 12 | 310 | 0.75 | 0.00 | 3.30 | 25.00 |
| 88 | 2 | 12 | 310 | 0.75 | 0.00 | 10.00 | 2.00 |
| 89 | 2 | 12 | 310 | 0.75 | 0.00 | 10.00 | 10.00 |

| | | | | | | | |
|---|---|---|---|---|---|---|---|
| 90 | 2 | 12 | 310 | 0.75 | 0.00 | 10.00 | 25.00 |
| 91 | 2 | 12 | 310 | 0.75 | 0.25 | 1.00 | 2.00 |
| 92 | 2 | 12 | 310 | 0.75 | 0.25 | 1.00 | 10.00 |
| 93 | 2 | 12 | 310 | 0.75 | 0.25 | 1.00 | 25.00 |
| 94 | 2 | 12 | 310 | 0.75 | 0.25 | 3.30 | 2.00 |
| 95 | 2 | 12 | 310 | 0.75 | 0.25 | 3.30 | 10.00 |
| 96 | 2 | 12 | 310 | 0.75 | 0.25 | 3.30 | 25.00 |
| 97 | 2 | 12 | 310 | 0.75 | 0.25 | 10.00 | 2.00 |
| 98 | 2 | 12 | 310 | 0.75 | 0.25 | 10.00 | 10.00 |
| 99 | 2 | 12 | 310 | 0.75 | 0.25 | 10.00 | 25.00 |
| 100 | 2 | 12 | 310 | 0.75 | 0.50 | 1.00 | 2.00 |
| 101 | 2 | 12 | 310 | 0.75 | 0.50 | 1.00 | 10.00 |
| 102 | 2 | 12 | 310 | 0.75 | 0.50 | 1.00 | 25.00 |
| 103 | 2 | 12 | 310 | 0.75 | 0.50 | 3.30 | 2.00 |
| 104 | 2 | 12 | 310 | 0.75 | 0.50 | 3.30 | 10.00 |
| 105 | 2 | 12 | 310 | 0.75 | 0.50 | 3.30 | 25.00 |
| 106 | 2 | 12 | 310 | 0.75 | 0.50 | 10.00 | 2.00 |
| 107 | 2 | 12 | 310 | 0.75 | 0.50 | 10.00 | 10.00 |
| 108 | 2 | 12 | 310 | 0.75 | 0.50 | 10.00 | 25.00 |
| 109 | 2 | 12 | 310 | 1.00 | 0.00 | 1.00 | 2.00 |
| 110 | 2 | 12 | 310 | 1.00 | 0.00 | 1.00 | 10.00 |
| 111 | 2 | 12 | 310 | 1.00 | 0.00 | 1.00 | 25.00 |
| 112 | 2 | 12 | 310 | 1.00 | 0.00 | 3.30 | 2.00 |
| 113 | 2 | 12 | 310 | 1.00 | 0.00 | 3.30 | 10.00 |
| 114 | 2 | 12 | 310 | 1.00 | 0.00 | 3.30 | 25.00 |
| 115 | 2 | 12 | 310 | 1.00 | 0.00 | 10.00 | 2.00 |
| 116 | 2 | 12 | 310 | 1.00 | 0.00 | 10.00 | 10.00 |
| 117 | 2 | 12 | 310 | 1.00 | 0.00 | 10.00 | 25.00 |

# APPENDIX B: DIAMOND-SHAPED WEC ARRAY MODEL SENSITIVITY PARAMETERS

| Run | Input $H_s$ (m) | Input $T_p$ (s) | Input MWD (deg) | Reflection Coefficient | Gamma – Freq Spreading | M – Dir Spreading (power) | Transmission Coefficient | # WEC Devices | Array Depth Contour(m) |
|---|---|---|---|---|---|---|---|---|---|
| 1 | 1.7 | 12.5 | 205 | 0 | 3.3 | 10 | 0.3 | 10 | 40 |
| 2 | 1.7 | 12.5 | 205 | 0 | 3.3 | 10 | 0.4 | 10 | 40 |
| 3 | 1.7 | 12.5 | 205 | 0 | 3.3 | 10 | 0.5 | 10 | 40 |
| 4 | 1.7 | 12.5 | 205 | 0 | 3.3 | 10 | 0.6 | 10 | 40 |
| 5 | 1.7 | 12.5 | 205 | 0 | 3.3 | 10 | 0.7 | 10 | 40 |
| 6 | 1.7 | 12.5 | 205 | 0 | 3.3 | 10 | 0.3 | 50 | 40 |
| 7 | 1.7 | 12.5 | 205 | 0 | 3.3 | 10 | 0.4 | 50 | 40 |
| 8 | 1.7 | 12.5 | 205 | 0 | 3.3 | 10 | 0.5 | 50 | 40 |
| 9 | 1.7 | 12.5 | 205 | 0 | 3.3 | 10 | 0.6 | 50 | 40 |
| 10 | 1.7 | 12.5 | 205 | 0 | 3.3 | 10 | 0.7 | 50 | 40 |
| 11 | 1.7 | 12.5 | 205 | 0 | 3.3 | 10 | 0.3 | 100 | 40 |
| 12 | 1.7 | 12.5 | 205 | 0 | 3.3 | 10 | 0.4 | 100 | 40 |
| 13 | 1.7 | 12.5 | 205 | 0 | 3.3 | 10 | 0.5 | 100 | 40 |
| 14 | 1.7 | 12.5 | 205 | 0 | 3.3 | 10 | 0.6 | 100 | 40 |
| 15 | 1.7 | 12.5 | 205 | 0 | 3.3 | 10 | 0.7 | 100 | 40 |
| 16 | 1.7 | 12.5 | 205 | 0 | 3.3 | 10 | 0.3 | 200 | 40 |
| 17 | 1.7 | 12.5 | 205 | 0 | 3.3 | 10 | 0.4 | 200 | 40 |
| 18 | 1.7 | 12.5 | 205 | 0 | 3.3 | 10 | 0.5 | 200 | 40 |
| 19 | 1.7 | 12.5 | 205 | 0 | 3.3 | 10 | 0.6 | 200 | 40 |
| 20 | 1.7 | 12.5 | 205 | 0 | 3.3 | 10 | 0.7 | 200 | 40 |
| 21 | 1.7 | 12.5 | 205 | 0 | 3.3 | 10 | 0.3 | 10 | 50 |
| 22 | 1.7 | 12.5 | 205 | 0 | 3.3 | 10 | 0.4 | 10 | 50 |
| 23 | 1.7 | 12.5 | 205 | 0 | 3.3 | 10 | 0.5 | 10 | 50 |
| 24 | 1.7 | 12.5 | 205 | 0 | 3.3 | 10 | 0.6 | 10 | 50 |
| 25 | 1.7 | 12.5 | 205 | 0 | 3.3 | 10 | 0.7 | 10 | 50 |
| 26 | 1.7 | 12.5 | 205 | 0 | 3.3 | 10 | 0.3 | 50 | 50 |
| 27 | 1.7 | 12.5 | 205 | 0 | 3.3 | 10 | 0.4 | 50 | 50 |
| 28 | 1.7 | 12.5 | 205 | 0 | 3.3 | 10 | 0.5 | 50 | 50 |
| 29 | 1.7 | 12.5 | 205 | 0 | 3.3 | 10 | 0.6 | 50 | 50 |
| 30 | 1.7 | 12.5 | 205 | 0 | 3.3 | 10 | 0.7 | 50 | 50 |
| 31 | 1.7 | 12.5 | 205 | 0 | 3.3 | 10 | 0.3 | 100 | 50 |
| 32 | 1.7 | 12.5 | 205 | 0 | 3.3 | 10 | 0.4 | 100 | 50 |
| 33 | 1.7 | 12.5 | 205 | 0 | 3.3 | 10 | 0.5 | 100 | 50 |
| 34 | 1.7 | 12.5 | 205 | 0 | 3.3 | 10 | 0.6 | 100 | 50 |
| 35 | 1.7 | 12.5 | 205 | 0 | 3.3 | 10 | 0.7 | 100 | 50 |
| 36 | 1.7 | 12.5 | 205 | 0 | 3.3 | 10 | 0.3 | 200 | 50 |
| 37 | 1.7 | 12.5 | 205 | 0 | 3.3 | 10 | 0.4 | 200 | 50 |
| 38 | 1.7 | 12.5 | 205 | 0 | 3.3 | 10 | 0.5 | 200 | 50 |
| 39 | 1.7 | 12.5 | 205 | 0 | 3.3 | 10 | 0.6 | 200 | 50 |
| 40 | 1.7 | 12.5 | 205 | 0 | 3.3 | 10 | 0.7 | 200 | 50 |

| | | | | | | | | | |
|---|---|---|---|---|---|---|---|---|---|
| 41 | 1.7 | 12.5 | 205 | 0 | 3.3 | 10 | 0.3 | 10 | 60 |
| 42 | 1.7 | 12.5 | 205 | 0 | 3.3 | 10 | 0.4 | 10 | 60 |
| 43 | 1.7 | 12.5 | 205 | 0 | 3.3 | 10 | 0.5 | 10 | 60 |
| 44 | 1.7 | 12.5 | 205 | 0 | 3.3 | 10 | 0.6 | 10 | 60 |
| 45 | 1.7 | 12.5 | 205 | 0 | 3.3 | 10 | 0.7 | 10 | 60 |
| 46 | 1.7 | 12.5 | 205 | 0 | 3.3 | 10 | 0.3 | 50 | 60 |
| 47 | 1.7 | 12.5 | 205 | 0 | 3.3 | 10 | 0.4 | 50 | 60 |
| 48 | 1.7 | 12.5 | 205 | 0 | 3.3 | 10 | 0.5 | 50 | 60 |
| 49 | 1.7 | 12.5 | 205 | 0 | 3.3 | 10 | 0.6 | 50 | 60 |
| 50 | 1.7 | 12.5 | 205 | 0 | 3.3 | 10 | 0.7 | 50 | 60 |
| 51 | 1.7 | 12.5 | 205 | 0 | 3.3 | 10 | 0.3 | 100 | 60 |
| 52 | 1.7 | 12.5 | 205 | 0 | 3.3 | 10 | 0.4 | 100 | 60 |
| 53 | 1.7 | 12.5 | 205 | 0 | 3.3 | 10 | 0.5 | 100 | 60 |
| 54 | 1.7 | 12.5 | 205 | 0 | 3.3 | 10 | 0.6 | 100 | 60 |
| 55 | 1.7 | 12.5 | 205 | 0 | 3.3 | 10 | 0.7 | 100 | 60 |
| 56 | 1.7 | 12.5 | 205 | 0 | 3.3 | 10 | 0.3 | 200 | 60 |
| 57 | 1.7 | 12.5 | 205 | 0 | 3.3 | 10 | 0.4 | 200 | 60 |
| 58 | 1.7 | 12.5 | 205 | 0 | 3.3 | 10 | 0.5 | 200 | 60 |
| 59 | 1.7 | 12.5 | 205 | 0 | 3.3 | 10 | 0.6 | 200 | 60 |
| 60 | 1.7 | 12.5 | 205 | 0 | 3.3 | 10 | 0.7 | 200 | 60 |

# DISTRIBUTION

4 Lawrence Livermore National Laboratory
Attn: N. Dunipace (1)
P.O. Box 808, MS L-795
Livermore, CA 94551-0808

1 MS0899 Technical Library 9536 (electronic copy)


Sandia National Laboratories